Molecular Cell

Article

SPARCLE, a p53-induced lncRNA, controls apoptosis after genotoxic stress by promoting PARP-1 cleavage

Graphical abstract

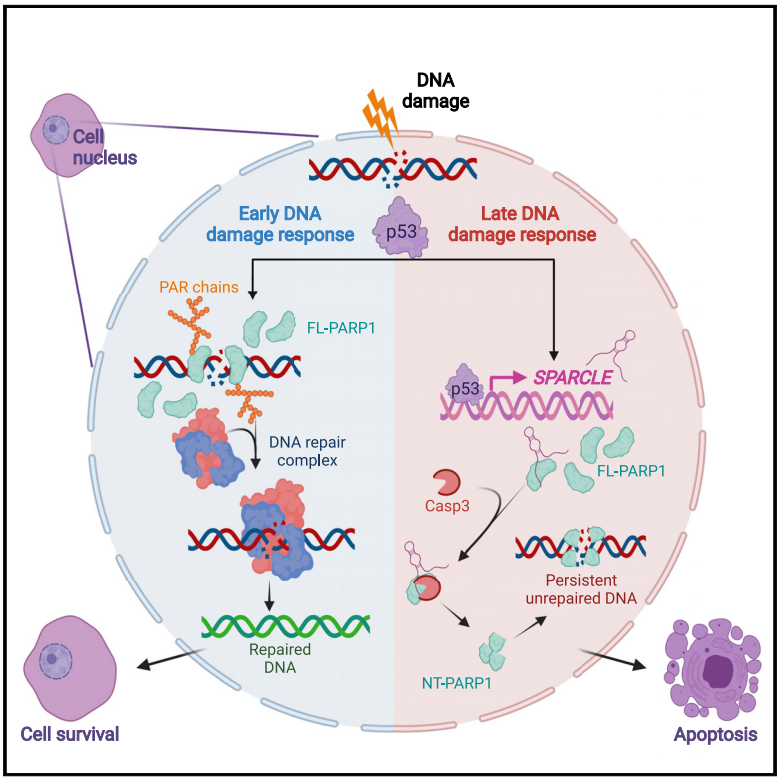

Highlights

- *SPARCLE* is a p53-induced, nuclear lncRNA that mediates DNA-damage-induced apoptosis
- *SPARCLE* inhibits repair of DNA single-stranded and double-stranded breaks
- *SPARCLE* binds to PARP-1 and promotes caspase-3 cleavage of PARP-1
- The N-terminal fragment of PARP-1 restores apoptosis in *SPARCLE*-deficient cells

Authors

Karla F. Meza-Sosa, Rui Miao, Francisco Navarro, ..., Ashish Lal, Hao Wu, Judy Lieberman

Correspondence

karla.meza@ibt.unam.mx (K.F.M.-S.), judy.lieberman@childrens.harvard.edu (J.L.)

In brief

Meza-Sosa et al. characterized a p53-regulated long non-coding RNA named *SPARCLE*. *SPARCLE* is needed to induce apoptosis by enhancing caspase-3-mediated PARP-1 cleavage in response to DNA damage.

Meza-Sosa et al., 2022, Molecular Cell *82*, 785–802
February 17, 2022
https://doi.org/10.1016/j.molcel.2022.01.001

CellPress

Molecular Cell

CellPress

Article

SPARCLE, a p53-induced lncRNA, controls apoptosis after genotoxic stress by promoting PARP-1 cleavage

Karla F. Meza-Sosa,[1,2,3,7,*] Rui Miao,[1,2,7] Francisco Navarro,[1,2,4,7] Zhibin Zhang,[1,2,8] Ying Zhang,[1,2] Jun Jacob Hu,[1,5] Corrine Corrina R. Hartford,[6] Xiao Ling Li,[6] Gustavo Pedraza-Alva,[3] Leonor Pérez-Martínez,[3] Ashish Lal,[6] Hao Wu,[1,5] and Judy Lieberman[1,2,9,*]

[1]Program in Cellular and Molecular Medicine, Boston Children's Hospital, Boston, MA 02115, USA
[2]Department of Pediatrics, Harvard Medical School, Boston, MA 02115, USA
[3]Laboratorio de Neuroinmunobiología, Departamento de Medicina Molecular y Bioprocesos, Instituto de Biotecnología, Universidad Nacional Autónoma de México, Cuernavaca, MOR 62210, México
[4]Bluebird Bio, Cambridge, MA 02142, USA
[5]Department of Biological Chemistry and Molecular Pharmacology, Harvard Medical School, Boston, MA 02115, USA
[6]Regulatory RNAs and Cancer Section, Genetics Branch, Center for Cancer Research (CCR), National Cancer Institute (NCI), National Institutes of Health (NIH), Bethesda, MD 20895, USA
[7]These authors contributed equally
[8]Present address: Department of Immunology, The University of Texas MD Anderson Cancer Center, Houston, TX 77030, USA
[9]Lead contact
*Correspondence: karla.meza@ibt.unam.mx (K.F.M.-S.), judy.lieberman@childrens.harvard.edu (J.L.)
https://doi.org/10.1016/j.molcel.2022.01.001

SUMMARY

p53, master transcriptional regulator of the genotoxic stress response, controls cell-cycle arrest and apoptosis following DNA damage. Here, we identify a p53-induced lncRNA suicidal PARP-1 cleavage enhancer (*SPARCLE*) adjacent to miR-34b/c required for p53-mediated apoptosis. *SPARCLE* is a ~770-nt, nuclear lncRNA induced 1 day after DNA damage. Despite low expression (<16 copies/cell), *SPARCLE* deletion increases DNA repair and reduces DNA-damage-induced apoptosis as much as p53 deficiency, while its overexpression restores apoptosis in p53-deficient cells. *SPARCLE* does not alter gene expression. *SPARCLE* binds to PARP-1 with nanomolar affinity and causes apoptosis by acting as a caspase-3 cofactor for PARP-1 cleavage, which separates PARP-1's N-terminal (NT) DNA-binding domain from its catalytic domains. NT-PARP-1 inhibits DNA repair. Expressing NT-PARP-1 in *SPARCLE*-deficient cells increases unrepaired DNA damage and restores apoptosis after DNA damage. Thus, *SPARCLE* enhances p53-induced apoptosis by promoting PARP-1 cleavage, which interferes with DNA-damage repair.

INTRODUCTION

p53 is the master transcriptional regulator of the cellular genotoxic stress response. Inactivating mutations of *TP53*, the gene encoding p53, occur in almost every type of cancer and are linked to poor prognosis. *TP53* is the most frequently mutated gene in cancer, indicating its potency as a tumor suppressor. Mice carrying inactivating *TP53* mutations develop tumors spontaneously within six months of birth. Depending on the severity of the stress and the target cell, p53 can promote cell repair and survival or cell-cycle arrest, senescence, or apoptosis by controlling the expression of both coding and non-coding RNAs (ncRNAs). p53 activates the transcription of over a hundred genes, including the CDK4/6 inhibitor *CDKN1A/p21*, to block cell-cycle progression and the bcl-2 family genes to promote apoptosis (Kastenhuber and Lowe, 2017; Lane, 1992; Vogelstein et al., 2000).

No single protein-coding p53 transcriptional target gene explains the strong effect of p53 on tumorigenesis and malignancy, prompting researchers to investigate p53-induced ncRNAs (Bieging-Rolett et al., 2020; Chaudhary and Lal, 2017; Dangelmaier et al., 2019; Grossi et al., 2016; Léveillé et al., 2015; Sánchez et al., 2014). The miR-34 microRNA (miRNA) family is the most studied p53-regulated ncRNA (He et al., 2007; Hermeking, 2007; Raver-Shapira et al., 2007). In humans, the miR-34 family has three members: miR-34a on chromosome 1 and miR-34b and miR-34c, located in the same transcriptional unit on chromosome 11 (Figure 1A). miR-34a is considered a tumor suppressor—its overexpression (OE) enhances p53-mediated cell-cycle arrest or apoptosis (Rokavec et al., 2014) and its expression is reduced in some cancers. The miR-34 family directly or indirectly suppresses many known p53-regulated genes. However, miR-34a deletion has minor effects on apoptosis and cell-cycle progression after genotoxic stress (Navarro and Lieberman, 2015)

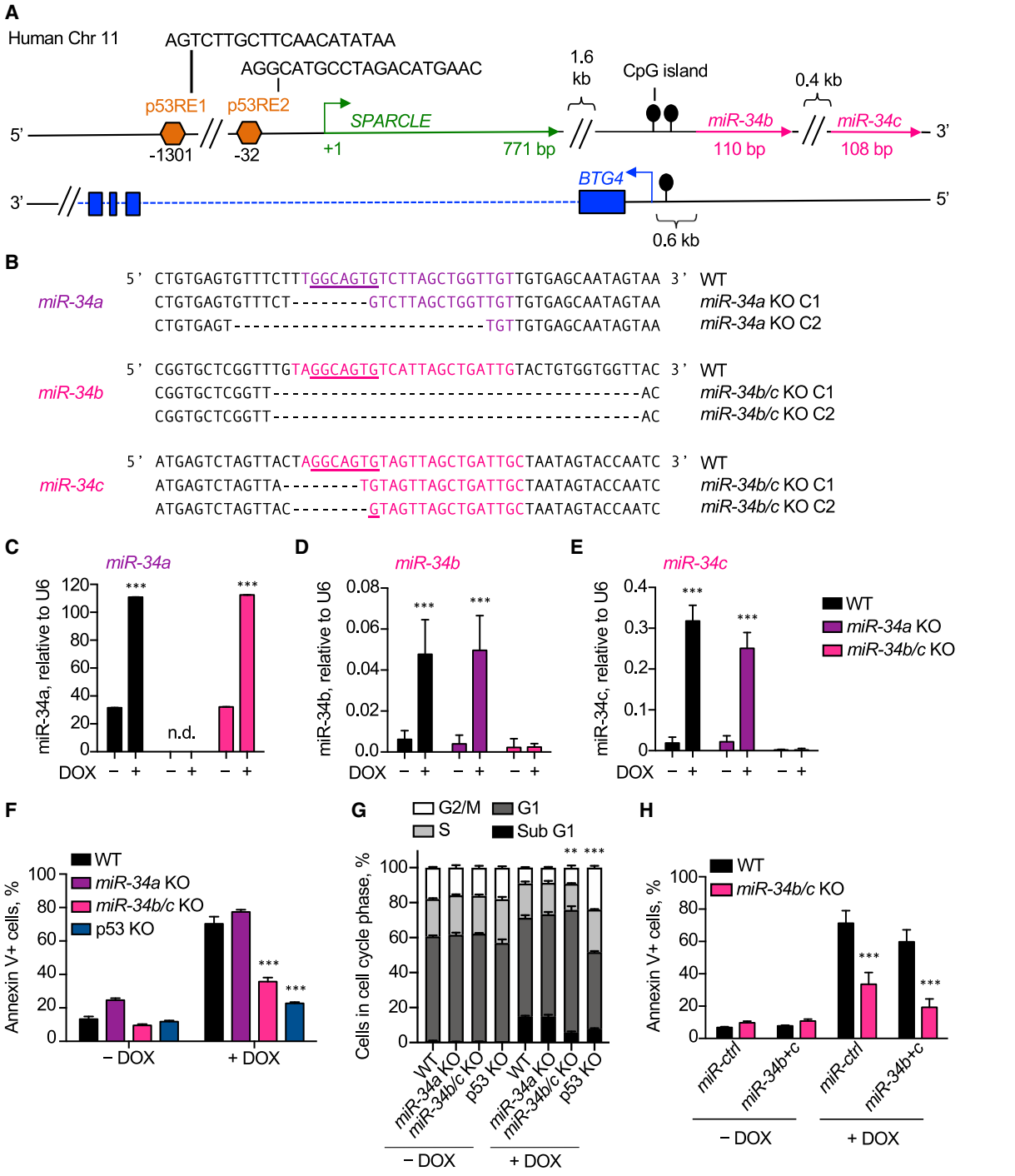

Figure 1. miR-34b/c knockout disrupts p53-mediated apoptosis after DNA damage

(A) miR-34b/c and *SPARCLE* genomic locus on human chromosome 11. The promoter contains two potential binding sites for p53 (p53RE1 and p53RE2). *BTG4* is on the opposite strand.

(B) miR-34a, miR-34b, and miR-34c TALEN-guided deletions in HCT116 used in this study.

(C–E) miR-34a (C) and miR-34b/c (D and E) expression analyzed by qRT-PCR in untreated and DOX-treated WT, miR-34a knockout (KO), and miR-34b/c KO HCT116.

(F and G) Untreated or DOX-treated WT, miR-34a KO, miR-34b/c KO, and p53 KO HCT116 analyzed by flow cytometry for annexin V staining (F) and cell-cycle profile (G) 48 h after treatment.

(legend continued on next page)

and does not cause a strong *in vivo* phenotype (Concepcion et al., 2012). This puzzling result might be explained if other miR-34 family members, miR-34b and miR-34c, substitute for miR-34a. However, genetic deletion of all 3 miR-34 miRNAs (Concepcion et al., 2012) in mice did not impair the p53 response to genotoxic damage or lead to an increase in spontaneous tumors within the first year of life, unlike haploinsufficiency or deletion of p53. Deletion of the miR-34 family and the 3 genes of the miR-449 family, which share a 7-nt seed sequence, profoundly impaired ciliogenesis, leading to respiratory dysfunction, infertility, and early mortality (Song et al., 2014). However, these problems were considered unrelated to p53.

To understand the lack of a strong miR-34a deletion phenotype and the functional redundancy of the miR-34 family, we generated miR-34b/c null HCT116. Unexpectedly, miR-34b/c deletion (unlike miR-34a deletion) reduced DNA-damage-induced apoptosis as much as p53 deficiency. However, expressing the deleted miRNAs did not rescue the phenotype, suggesting that something other than miR-34b/c deficiency was responsible. Here, we show that a lncRNA adjacent to the miR-34b/c cluster that we named suicidal PARP-1 cleavage enhancer (*SPARCLE*), which is not expressed in miR-34b/c-deleted cells and is induced late after DNA damage by p53 binding to a p53 response element (p53RE) that also induces miR-34b/c, regulates apoptosis after DNA damage. Cells genetically deficient in miR-34b/c, *SPARCLE*, or the p53RE that controls miR-34b/c and *SPARCLE* expression phenocopy the lack of DNA-damage-induced cell death as strongly as p53-deficient cells. Even though *SPARCLE* expression is delayed and low after DNA damage, it powerfully promotes apoptosis in cells with unrepaired DNA damage by inhibiting late DNA-damage repair.

RESULTS

miR-34b/c knockout cells are resistant to DNA-damage-induced apoptosis

To investigate whether the lack of a DNA-damage phenotype in miR-34a knockout (KO) cells and mice could be due to redundancy of other family members (miR-34b and miR-34c), HCT116 cells deficient in miR-34a or miR-34b and miR-34c were generated using transcription-activator-like effector nucleases (TALENs) (Figure 1B). As expected, each of these miRNAs was induced by doxorubicin (DOX) in wild-type (WT) HCT116 cells, but not in cells in which the corresponding miRNA gene was deleted (Figures 1C–1E) or in p53 hypomorphic cells (Figure S1A). As previously reported, miR-34a deletion did not affect basal or DNA-damage-induced apoptosis or cell-cycle profile (Navarro and Lieberman, 2015), in contrast to p53 hypomorphic cells (Bunz et al., 1999) (referred to hereafter as p53 KO cells) that showed greatly reduced sub G1 cells, a sign of apoptosis, after DOX (Figures 1F and 1G). Deletion of miR-34b and miR-34c reduced DOX-induced apoptosis almost as much as p53 KO (Figure 1F), resulting in fewer sub G1 cells, and an increase in arrested cells. No cell-cycle profile change was observed under basal conditions, but DOX-treated miR-34b/c KO cells had increased G1 cells (Figure 1G). To determine whether the apoptotic defect in miR-34b/c KO cells was due to miR-34b/c, miR-34b and miR-34c mimics were transfected into miR-34b/c KO HCT116. Surprisingly, mature miR-34b and miR-34c mimics did not rescue apoptosis of miR-34b/c KO cells, suggesting that lack of these two miRNAs was not responsible for protection from apoptosis (Figure 1H).

SPARCLE is a ~770-nt nuclear lncRNA

Reduced apoptosis in damaged miR-34b/c KO cells might be caused by off-target TALEN disruption of another gene or effects of miR-34b/c disruption on expression of a nearby gene on human chromosome 11. Multiple miR-34b/c KO clones had the same phenotype (data not shown), suggesting that an off-target deletion was not responsible for the loss of DNA-damage-induced apoptosis. 3-kb upstream of the miR-34b/c pre-miRNA sequence, a putative non-conserved lncRNA named *LOC728196* was annotated (Figure 1A). *LOC728196* was intermittently removed from public databases, raising questions about whether it is a *bona fide* lncRNA. However, a previous report confirmed *LOC728196* expression by qRT-PCR in some glioma and astrocytoma cell lines and linked high expression in glioma to poor prognosis (Wang et al., 2018). For reasons that will be explained later, we renamed this putative lncRNA *SPARCLE*. *SPARCLE*'s expression was not detected above background by qRT-PCR under basal conditions in WT and p53 KO HCT116 but was induced after DOX treatment only in p53 WT cells (Figure 2A). Expression was first detected 24 h after DOX at a low level (mean ~1 copy/cell) and further increased to a mean of ~8 copies/cell by 48 h. *SPARCLE* was not detected in untreated, p53 KO or miR-34b/c KO cells (Figure 2A).

Because the size and properties of the *SPARCLE* transcript are not known, we characterized it further. 5′ rapid amplification of cDNA ends (RACE) was used to define the *SPARCLE* transcription start site (TSS) (Figure 2B). Two TSS's located 29-nt (TSS1) and 14-nt (TSS2) downstream of the annotated *LOC728196* TSS were cloned at equal frequencies (Figure S1B). In this paper TSS1 coordinates will be arbitrarily used for annotation. To define the length of *SPARCLE*, we tried different approaches. *SPARCLE* was not detected by northern blot even after DNA damage or by 3′ RACE (data not shown). Since 3′ RACE relies on poly(A) tails to amplify 3′-ends, *SPARCLE* may not be polyadenylated. Circular RACE, which does not depend on polyadenylation for amplification, amplified a reproducible and strong signal, which was cloned and sequenced (Figure 2C). None of the sequences had a poly(A) tail. All the clones ended 771 nt downstream of TSS1. Thus, *SPARCLE* is a ~770 nt lncRNA that likely is not polyadenylated (Figure S1C).

Next, we assessed whether *SPARCLE*'s sequence is conserved upstream of miR-34b/c in other species (Figure S1D).

(H) WT and miR-34b/c KO HCT116 transfected with a control miRNA (miR-ctrl) or co-transfected with miR-34b and miR-34c mimics were untreated or treated with DOX for 48 h and analyzed for annexin V staining by flow cytometry.

All graphs show mean ± SEM of 3 technical replicates and are representative of at least 3 independent experiments. In (C–E) two-tailed t tests compared with no DOX (C–E) or WT (F and H). (G) Cell-cycle differences were analyzed by one-way ANOVA using the Holm-Sidak method. *$p < 0.05$, **$p < 0.01$, ***$p < 0.001$; comparing −DOX and +DOX (C–E) or versus WT (F–H).

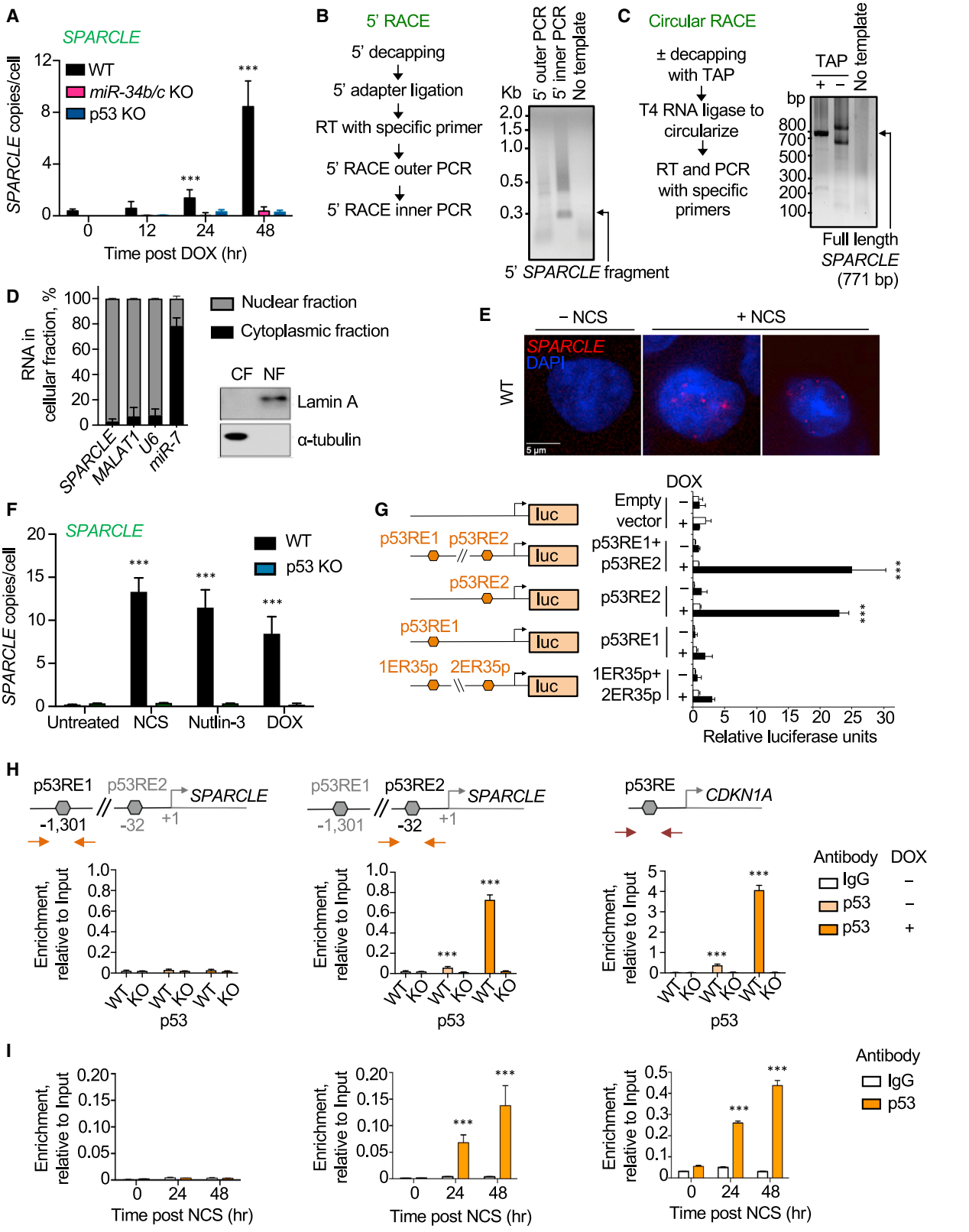

(legend on next page)

SPARCLE is well conserved among primates and some other mammals, including cow, sheep, and pig, with identities of 80%–95% in ~40% of the 771 nt *SPARCLE* sequence. A similar large region is not well conserved in rodents; however, a ~150-nt region immediately downstream of TSS1 is highly conserved (>70%) in all mammals analyzed, suggesting that this region may be functional. A conserved sequence upstream of the miR-34b/c cluster was not found in fish, reptiles, or any invertebrates. A sequence analysis using the coding potential calculator (CPC) versions 1 and 2 (Kang et al., 2017) indicated that *SPARCLE* is unlikely to be translated (CPC1 coding potential, −1.319; CPC2 coding probability, 0.0093). Thus, *SPARCLE* is a bona fide mammalian lncRNA.

To determine *SPARCLE*'s cellular localization, WT HCT116 cells were separated into nuclear and cytoplasmic fractions (CFs) 48 h after DOX treatment, and RNA was extracted from each fraction and analyzed by qRT-PCR for *SPARCLE*. Two nuclear ncRNAs, *MALAT1* and *U6*, and the cytoplasmic miRNA miR-7 were amplified as controls (Figure 2D). *SPARCLE* was only detected in the nuclear fraction (NF), while the other transcripts were localized as expected. To confirm *SPARCLE*'s nuclear localization, single-molecule RNA fluorescence *in situ* hybridization (smFISH) (Orjalo et al., 2011; Raj et al., 2008) was performed using *SPARCLE* probes in WT HCT116 48 h after adding medium or the double-strand DNA break (DSB)-inducing agent neocarzinostatin (NCS). *SPARCLE* was not detected in unstressed cells, but nuclear puncta were observed in NCS-treated cells (Figure 2E). No signal was detected in NCS-treated *SPARCLE* KO cells (see below), indicating that the smFISH assay was specific (Figure S1E). Thus, *SPARCLE* is a low abundance, DNA-damage-induced, nuclear lncRNA.

SPARCLE's promoter contains one functional p53 response element

Just 5′ to *SPARCLE*'s TSS1 are two predicted p53REs, p53RE1 (beginning at −1,301 nt) and p53RE2 (at −32 nt). To determine whether *SPARCLE* is induced by p53, its expression was analyzed in p53 KO and WT HCT116 cells treated with the DNA-damaging agents DOX and NCS or nutlin-3, an Mdm2 inhibitor that activates p53 without causing genotoxic stress. As expected, *SPARCLE* was detected after all these p53-activating stimuli, but only in p53-sufficient cells (Figure 2F). Thus, p53 activation is all that is needed to induce *SPARCLE*. To determine whether the two putative p53REs upstream of *SPARCLE*'s TSS are functional, the complete region that contains one or both p53REs or the complete region in reverse orientation (1ER35p + 2ER35p) were cloned upstream of a luciferase reporter gene. HCT116 were transfected with these reporter plasmids, treated or not with DOX, and assessed for luciferase activity 48 h later (Figure 2G). Luciferase activity was detected only after DOX in cells transfected with the p53RE1 + p53RE2 or p53RE2 reporters, indicating that p53RE2 is the only functional p53RE. To corroborate this finding, chromatin immunoprecipitation (ChIP) assays were performed using a p53 antibody or control IgG in WT and p53 KO HCT116 (Figure 2H). p53 bound to p53RE2 to a limited extent in untreated cells, but binding increased dramatically after DOX. Similarly, NCS treatment of WT HCT116 showed time-dependent binding of p53 to the p53RE2 beginning 24 h and increasing by 48 h after adding NCS (Figure 2I). p53 did not bind to p53RE1 after DNA damage. As positive control, p53 binding to the promoter of the p53 target gene *CDKN1A/p21* was verified. To examine whether p53-dependent upregulation of *SPARCLE* after DNA damage occurs in other cells, p53 was knocked down or not in lung adenocarcinoma (A549), hepatocellular carcinoma (HepG2), and poorly differentiated colon carcinoma (RKO), and the knocked down or control cells were treated or not with DOX. *SPARCLE*, *TP53/p53*, and *CDKN1A/p21* expression levels were measured by qPCR 24 h later (Figure S2). *SPARCLE* and *CDKN1A* were significantly upregulated in all three DOX-treated cell lines knocked down with a control siRNA, but their induction was strongly suppressed when p53 was knocked down (Figure S2). Thus, *SPARCLE* is a p53-induced lncRNA induced at low levels after genotoxic stress.

Cells lacking p53RE2 resist DNA-damage-induced apoptosis that is rescued by *SPARCLE* overexpression

Since *SPARCLE*'s induction depends on p53 binding to p53RE2, p53RE2 KO HCT116 clones were generated using TALENs to further investigate the role of *SPARCLE* in DNA-damage induced

Figure 2. *SPARCLE* is a p53-induced ~770-nt nuclear lncRNA

(A) *SPARCLE* expression analyzed by qPCR in DOX-treated WT, miR-34b/c KO, and p53 KO HCT116 at indicated times after adding DOX.

(B and C) *SPARCLE* transcription start site (TSS) and length (771 nt) determined by 5′ rapid amplification of cDNA ends (RACE) (B) and circular RACE (C), respectively. Shown are the experimental workflow (left) and agarose gel of the PCR products that were cloned and sequenced (right). Experiments performed using nuclear RNA 48 h after DOX treatment of WT HCT116. See also Figures S1B and S1C.

(D) RNA, extracted from fractionated WT HCT116 48 h after DOX treatment, was analyzed by qRT-PCR for the indicated ncRNAs. *MALAT1* and *U6* are nuclear and miR-7 is predominantly cytoplasmic. Lamin A and α-tubulin immunoblots of fractionated cells (right, nuclear fraction (NF), cytoplasmic fraction (CF)) assessed cell fractionation.

(E) WT HCT116 that were untreated or treated for 48 h with neocarzinostatin (NCS) probed for *SPARCLE* using single-molecule RNA FISH (red). Nuclear DNA labeled with DAPI (blue). See also Figure S1E.

(F) *SPARCLE* measured by qRT-PCR after 48 h incubation with NCS, nutlin-3 or DOX in WT and p53 KO HCT116.

(G) p53 promoter reporter assay. Luciferase activity of untreated or DOX-treated WT HCT116 that had been transfected with empty vector or luciferase reporters containing p53RE1 and/or p53RE2 p53 response elements or both in antisense orientation (2ER35p + 1ER35p) for 24 h. Luciferase activity measured 48 h after DOX.

(H and I) p53 chromatin immunoprecipitation (ChIP). Untreated or DOX-treated WT and p53 KO (H) or NCS-treated WT (I) HCT116 analyzed for p53 binding to p53REs within the promoters of *SPARCLE* (p53RE1 (left), p53RE2 (middle)), and *CDKN1A/p21* (right). ChIP performed 48 h (H) or at the indicated times (I) after treatment.

Graphs show mean ± SEM of 3 technical replicates, and data are representative of at least 3 independent experiments; ***$p < 0.001$ by two-tailed t test; comparing WT and p53 KO (A and F), −DOX and +DOX (G), and p53 antibody to control IgG (H and I).

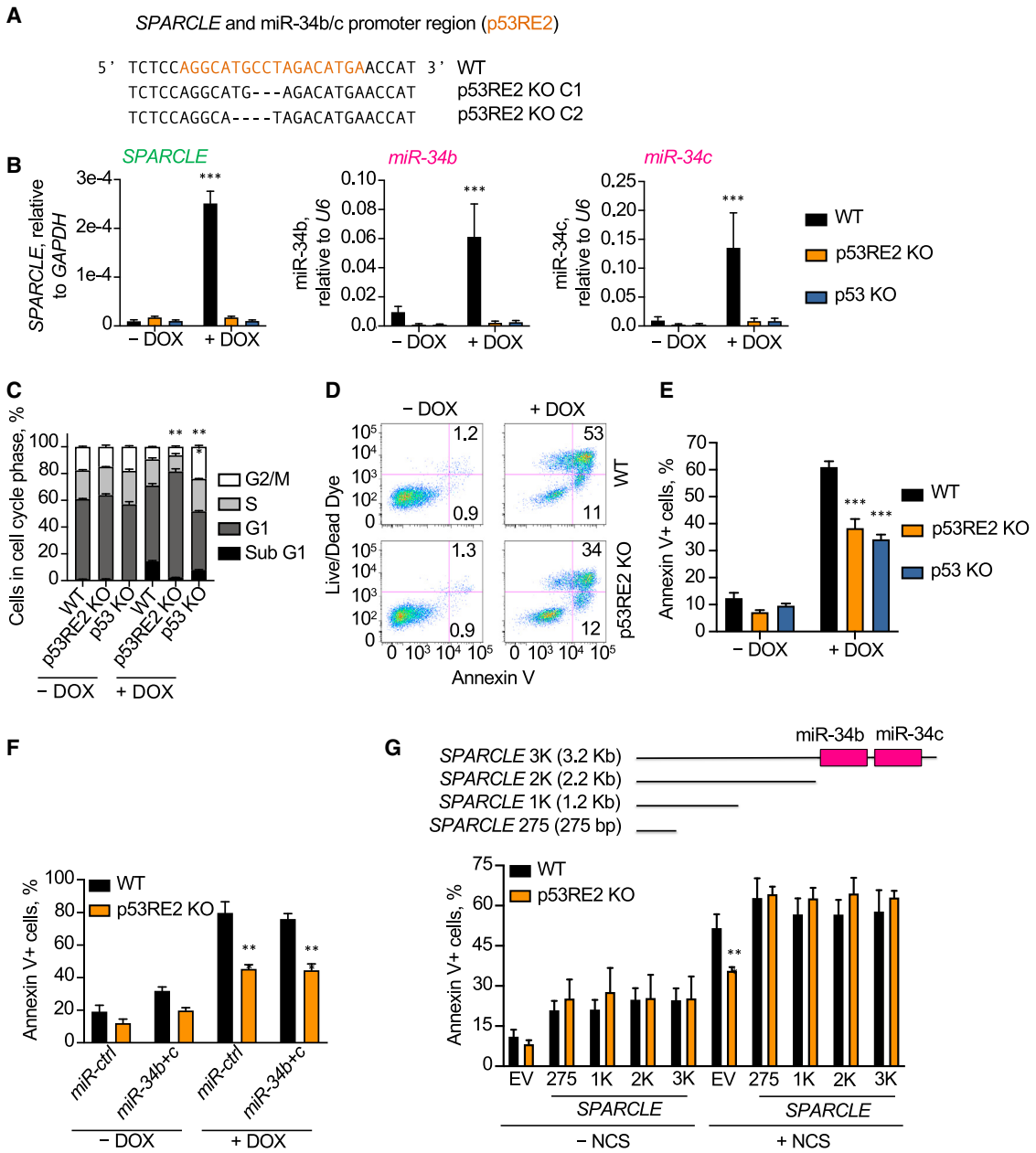

Figure 3. p53RE2 deletion phenocopies the apoptosis defect of p53 KO cells and is rescued by *SPARCLE*

(A) Sequence of the *SPARCLE* promoter region in two clones of p53RE2 KO compared with WT HCT116. The p53RE is orange.

(B) *SPARCLE* (left), miR-34b (middle) and miR-34c (right) expression, relative to *GAPDH* (left) or *U6* (middle and right), by qRT-PCR in untreated and DOX-treated WT, p53RE2 KO, and p53 KO HCT116.

(C–E) Cell-cycle profile (C) and annexin V staining (D, representative dot plot; E, mean ± SEM) by flow cytometry in untreated and DOX-treated WT, p53RE2 KO, and p53 KO HCT116.

(F–G) Annexin V staining by flow cytometry in WT and p53RE2 KO HCT116 that were transfected with a control miRNA (miR-ctrl), or with miR-34b and miR-34c mimics (F) or transfected with expression vectors containing indicated *SPARCLE* truncations (G) and then untreated or treated with DOX or NCS.

Cells analyzed 48 h after adding DOX or NCS. Graphs show mean ± SEM of 3 technical replicates, and data are representative of at least 3 independent experiments; $^{**}p < 0.01$, $^{***}p < 0.001$ by two-tailed t test, comparing −DOX and +DOX (B) or WT with KO cell lines (C and E–G). Cell-cycle differences were analyzed by one-way ANOVA using the Holm-Sidak method.

apoptosis (Figure 3A). Two clones were generated that behaved similarly (data not shown). As expected, deleting p53RE2 abrogated p53 binding to *SPARCLE*'s promoter (data not shown) and *SPARCLE* expression after genotoxic stress (Figure 3B, left). Deleting p53RE2 also blocked DOX-induced miR-34b/c (Figure 3B, middle and right), suggesting that *SPARCLE* and

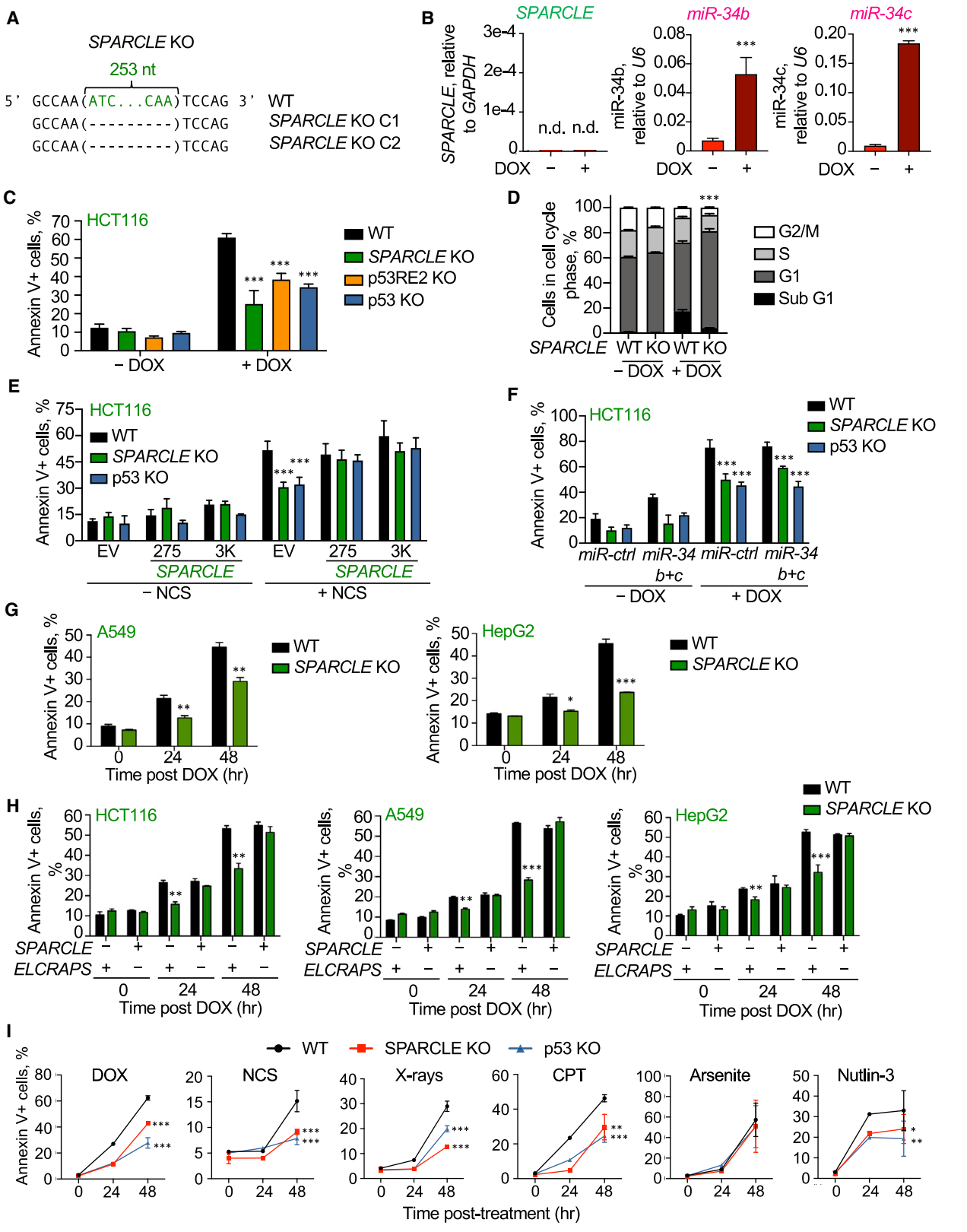

(legend on next page)

miR-34b/c are co-regulated or may form part of the same transcriptional unit. p53RE2 deficient cells did not have a significantly altered cell-cycle profile under basal conditions (Figure 3C). DOX treatment of p53RE2-deficient HCT116 cells, like miR34b/c KO cells (Figures 1F and 1G), reduced annexin V staining and apoptosis and increased G1 arrest compared with WT HCT116 (Figures 3C–3E). Moreover, p53RE2 deletion and p53 KO reduced DOX-induced apoptosis in HCT116 similarly.

Because p53RE2 deletion abrogates both *SPARCLE* and miR-34b/c expression, to determine which of these transcripts is responsible for promoting apoptosis, we performed rescue experiments. As before, transfection of miR-34b and miR-34c mimics did not increase apoptosis in p53RE2-deficient cells (Figure 3F). However, transfection of plasmids encoding different length *SPARCLE* constructs into p53RE2 KO HCT116 restored NCS-induced apoptosis to the level in WT HCT116 (Figure 3G). *SPARCLE* constructs encoding the first 275 bases, 1.2, 2.2, and 3.2 kb after *SPARCLE*'s TSS all restored apoptosis comparably. Thus, *SPARCLE* is needed for apoptosis and the first 275 bases of *SPARCLE* is active. Since *SPARCLE* KO-associated resistance to apoptosis was rescued by an exogenous plasmid, *SPARCLE* is likely a *trans*-acting lncRNA rather than a local chromatin modifier.

SPARCLE deficiency reduces apoptosis in response to DNA damage

To confirm the critical role of the 5′-end of *SPARCLE* in DNA-damage-induced apoptosis, HCT116 that lack the first 253 nt of *SPARCLE* (called *SPARCLE* KO) were generated using CRISPR-Cas9n (Figure 4A). Two KO clones gave similar results (data not shown). *SPARCLE* was not detected in *SPARCLE* KO cells even after DOX (Figure 4B, left), but both miR-34b and miR-34c were expressed without significant change compared with WT HCT116 (Figure 4B, middle and right). After DOX, apoptosis—assessed by annexin V staining 48 h later—was reduced compared with WT HCT116 to the same extent in *SPARCLE* KO, p53RE2 KO, and p53 KO HCT116 (Figure 4C). As previously observed for miR-34b/c KO and p53RE2 KO cells, *SPARCLE* KO had no significant effect on cell-cycle profile under basal conditions but showed fewer subG1 and increased G1 phase arrested cells after DOX (Figure 4D). Moreover, OE of either 275 nt or 3 kb *SPARCLE* comparably restored NCS-induced apoptosis in both *SPARCLE* KO and p53 KO cells (Figure 4E). The *SPARCLE* 3-kb construct contains the miR-34b/c precursor sequence, but the shorter 275-nt *SPARCLE* (*SPARCLE 275*) does not (Figure 3G). Nonetheless, expression of both constructs caused similar amounts of DNA-damage-induced apoptosis (Figure 4E). Moreover, transfection of miR-34b and miR-34c mimics did not rescue DNA-damage-induced apoptosis in *SPARCLE* KO or p53 KO cells (Figure 4F).

To examine whether *SPARCLE* regulated DNA-damage-induced apoptosis in other cells, *SPARCLE* KO clones were generated in two additional p53-sufficient cell lines—A549 and HepG2 (Figures S3A and S3B, left). As for HCT116, *SPARCLE* KO eliminated DOX-induced *SPARCLE* expression, but both miR-34b and miR-34c were induced by DOX in *SPARCLE* KO cells (Figures S3A and S3B, middle and right). *SPARCLE* KO dramatically reduced apoptosis in DOX-treated A549 and HepG2 (Figure 4G). Ectopic expression of *SPARCLE 275*, but not a 275-nt control RNA, transcribed from the opposite strand of *SPARCLE* (named *ELCRAPS*), in *SPARCLE* KO cells (Figure S3C), completely rescued DOX-induced apoptosis in all three *SPARCLE* KO lines (Figure 4H). In these experiments, ectopic *SPARCLE* and *ELCRAPS* were similarly overexpressed to ~40 copies/cell, which was modestly more than *SPARCLE* levels induced after DOX in WT cells (~8–16 copies/cell) (Figure S3C). Transfection of *SPARCLE* or *ELCRAPS* had no effect on miR-34b or miR-34c expression at baseline or after DOX (Figures S3D and S3E). Thus, *SPARCLE*, but not miR-34b/c, activates DNA-damage- and p53-induced apoptosis in multiple cell types.

SPARCLE promotes apoptosis in response to single- and double-stranded DNA damage

Until now, DNA damage was induced using two DSB-inducing agents, DOX or NCS, with similar results. To determine whether *SPARCLE* plays a role in other types of DNA damage, WT, *SPARCLE* KO, and p53 KO HCT116 were treated with a variety of agents that induce genotoxic stress or with nutlin-3, which activates a p53 response and caspase-3 independently of DNA damage. Apoptosis was measured by annexin V staining 24 and 48 h later (Figure 4I). Apoptosis in response to nutlin-3 or agents that cause DSB (DOX, NCS, and X-rays) or single-strand breaks (SSB) (camptothecin [CPT]) was strongly inhibited to a similar extent in *SPARCLE* KO and p53 KO HCT116 compared with WT HCT116. However, apoptosis in response to arsenite, which causes oxidative damage to DNA and abasic sites, was comparable in WT, p53 KO, and *SPARCLE* KO HCT116. Thus, *SPARCLE* plays a major role in p53-mediated apoptosis in response to both SSB and DSB but may not be important in responding to oxidative DNA damage.

Figure 4. *SPARCLE* deletion phenocopies the apoptosis defect of p53 KO cells and is rescued by *SPARCLE*

(A) CRISPR-Cas9n deletions of the 5′ region of *SPARCLE* in two independent HCT116 clones.

(B) *SPARCLE* (left), miR-34b (middle) and miR-34c (right) levels of untreated and DOX-treated *SPARCLE* KO HCT116 by qPCR. N.D., not detected.

(C and D) Annexin V staining (C) and cell-cycle profile (D) by flow cytometry of untreated and DOX-treated WT, *SPARCLE* KO, p53RE2 KO, and p53 KO HCT116.

(E and F) Annexin V staining by flow cytometry of untreated or DOX- or NCS-treated WT, *SPARCLE* KO and p53 KO HCT116 transfected with expression vectors containing indicated *SPARCLE* truncations (E) or transfected with a control miRNA (miR-ctrl), or with miR-34b and miR-34c mimics (F).

(G) Annexin V staining by flow cytometry of WT and *SPARCLE* KO A549 (left) and HepG2 (right) at indicated times after adding DOX.

(H) Annexin V staining by flow cytometry of untreated or DOX-treated WT and *SPARCLE* KO HCT116 (left), A549 (middle), and HepG2 (right), transfected to express *SPARCLE 275* or *ELCRAPS*.

(I) Annexin V staining by flow cytometry of WT, *SPARCLE* KO, and p53 KO HCT116 treated with indicated DNA-damaging agents or nutlin-3.

In (B–F), cells were analyzed 48 h after DOX or NCS. Graphs show mean ± SEM of 3 technical replicates, and data are representative of at least 3 independent experiments. In (B, C, and E–H) two-tailed t tests compared −DOX and +DOX (B) or WT with KO cell lines. In (D and I), differences between cell lines were analyzed by one-way ANOVA using the Holm-Sidak method for multiple comparisons. *$p < 0.05$, **$p < 0.01$, ***$p < 0.001$.

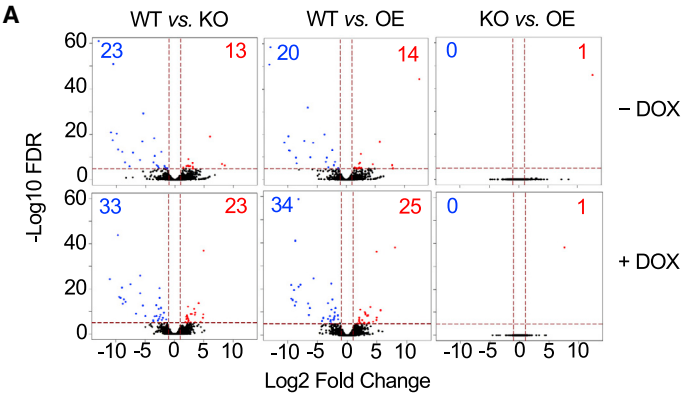

B

RAP-MS/WB

UV crosslink
↓
Nuclear extract
↓
Hybridization of biotinylated probes
↓
Capture with streptavidin beads
↓
RNA and DNA digestion to isolate RNA-bound proteins
↓
Mass spectrometry or western blot

C

Protein name	Unique peptides	Coverage, %	Molecular weight (kDa)
ILF3	23	30.40	95.28
HSPA8	22	30	70.85
PARP1	23	25.30	113.01
SF3B3	22	24.90	135.49
Ku80 (XRCC5)	13	24.20	82.65
SUPT16H	22	22.20	119.84
FASN	35	20.20	273.25
PRPF8	43	19.80	273.43
PRKDC (XRCC7)	70	17.90	468.79
SNRNP200	33	17.50	244.35

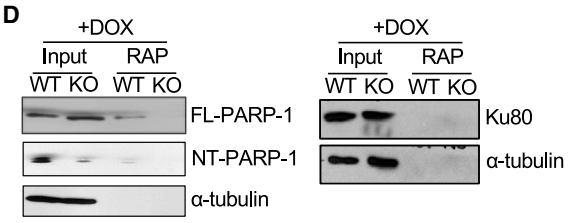

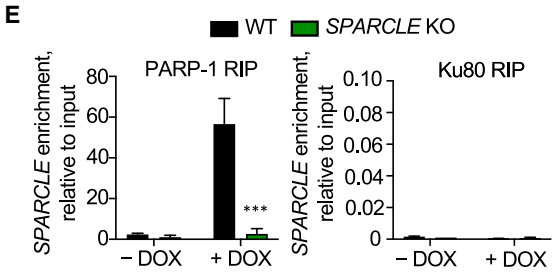

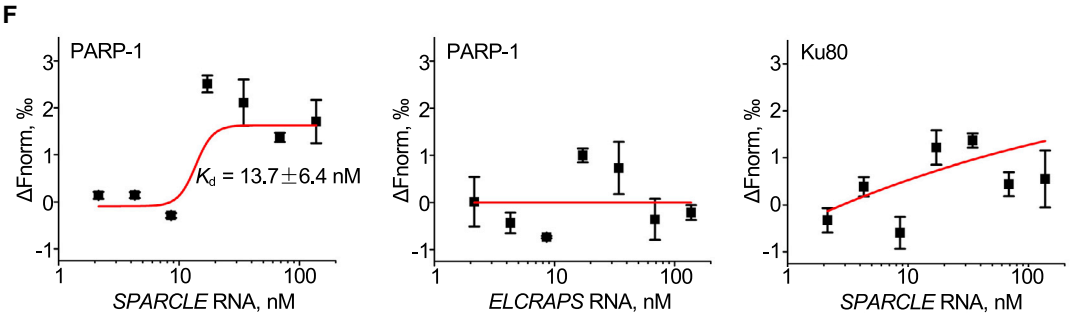

Figure 5. *SPARCLE* does not affect gene expression but interacts with DNA repair proteins

(A) Volcano plots showing few significant differentially expressed genes comparing duplicate samples of WT, *SPARCLE* KO (KO), and *SPARCLE* overexpressing (OE) HCT116 before and after DOX. Blue genes are significantly downregulated; red genes, upregulated. Dotted lines indicate 1 $\log_2$ fold change and FDR < 1e−5. See also Figure S4.

(B and C) *SPARCLE* RNA antisense purification-mass spectrometry (RAP-MS) experimental scheme (B) and 10 *SPARCLE*-interacting proteins with greatest peptide coverage isolated from nuclei of DOX-treated WT HCT116 (C).

(legend continued on next page)

SPARCLE does not regulate gene expression

Most nuclear lncRNAs whose function has been defined act as chromatin or transcription regulators (Huarte, 2015; Ulitsky and Bartel, 2013). To determine if *SPARCLE* regulates gene expression, RNA-seq of WT, *SPARCLE* KO, and *SPARCLE* KO overexpressing *SPARCLE 275* (*SPARCLE* OE) HCT116 that were untreated or treated with DOX for 48 h was compared in duplicate samples. As expected, DOX altered the expression of about a thousand genes, including well-known p53-regulated genes (Figures S4A–S4C; Table S1). However, surprisingly, when basal and DOX-induced gene expression were compared in WT, *SPARCLE* KO and *SPARCLE* OE cells, there were few consistent changes that could be linked to *SPARCLE* (Figures 5A and S4B). Similar results were found when the arbitrary threshold chosen to identify differentially expressed genes was changed. In fact, the expression profile of *SPARCLE* KO and OE cells were virtually identical. Moreover, *SPARCLE* KO did not significantly alter the basal or NCS-induced expression of *TP53*, *BTG4* (the nearby coding gene in the same locus), *PARP1* or key p53-induced genes, including *CDKN1A, BAX*, and *NOXA*, as measured by qRT-PCR (Figure S4D). Thus, *SPARCLE* is not a transcriptional regulator.

SPARCLE binds to PARP-1

To get a clue to how *SPARCLE* functions, RNA antisense purification-mass spectrometry (RAP-MS) (Engreitz et al., 2013; McHugh et al., 2015) was performed to pull down *SPARCLE*-interacting proteins from nuclei of DOX-treated WT and *SPARCLE* KO HCT116 (Figure 5B). Three 5′ biotinylated probes, antisense to the functional first 275 nt of *SPARCLE*, were used for pull-down (Table S3). 557 proteins with a minimum of 3 unique peptides were pulled down and identified in WT cells, and only 5 were found in *SPARCLE* KO cells, indicating assay specificity for identifying candidate *SPARCLE*-interacting proteins (Table S2). After filtering the 557 proteins based on their percent coverage ($\geq$17%), 206 proteins were chosen as candidate *SPARCLE* interactors. Among these, multiple proteins involved in the DNA-damage response (DDR) (PARP-1, Ku80/XRCC5, PRKDC/XRCC7/DNA-PK$_{CS}$) and splicing (SF3B3, PRPF8, SNRNP200) were found. Others included ILF3/NF90, the larger subunit of the NFAT transcription factor, which interacts with DNA-PK$_{CS}$ (Ting et al., 1998); the heat shock protein HSPA8; SUPT16H, a histone chaperone in the FACT chromatin remodeling complex; and the fatty acid synthase (FASN) (Figure 5C).

Because cells lacking *SPARCLE* are defective in DNA-damage-induced apoptosis, we focused on PARP-1, Ku80, and DNA-PK$_{CS}$, which sense DNA breaks and assemble on and repair damaged DNA (Ceccaldi et al., 2016; Spagnolo et al., 2012). In particular, PARP-1 senses and binds to both SSB and DSB and rapidly catalyzes PARylation, the addition of poly(-ADP) ribose (PAR) to recruit DNA repair factors to sites of DNA damage (Beck et al., 2014; Wei and Yu, 2016). When DNA damage is low, PARP-1 enhances survival (D'Amours et al., 2001; Halappanavar et al., 1999; Oliver et al., 1998). However, when damage is extensive, PARP-1 promotes apoptosis (D'Amours et al., 2001; Halappanavar et al., 1999; Oliver et al., 1998). Ku80 and DNA-PK$_{CS}$ are key factors in DSB repair by non-homologous end joining (NHEJ) (Ceccaldi et al., 2016; Chang et al., 2017; Li and Xu, 2016).

RNA antisense pull-down followed by western blot (RAP-WB) was used to assess the candidate *SPARCLE*-interacting DDR proteins identified by RAP-MS. RAP-WB confirmed an interaction of *SPARCLE* with both full-length (FL) and the caspase-3-cleaved N-terminal (NT) fragment of PARP-1 in WT cells. No signal was detected in *SPARCLE* KO HCT116 harvested 48 h after DOX (Figure 5D). DNA-PK$_{CS}$ was not detected in the input cell lysates (data not shown), and Ku80 was not detected in the RAP-WB (Figure 5D). qRT-PCR amplified *SPARCLE* in RNA immunoprecipitated (RIP) using PARP-1 antibody, but not using anti-Ku80 (Figure 5E). *SPARCLE* was not amplified in *SPARCLE* KO HCT116 or in untreated WT HCT116, confirming the specificity of the RIP assay. These data suggest that *SPARCLE* binds to PARP-1.

Microscale thermophoresis (MST) confirmed the interaction between *SPARCLE* and PARP-1. Alexa647-labeled human recombinant PARP-1 (R-PARP-1) or Ku80 were incubated with *in vitro* transcribed *SPARCLE 275* or *ELCRAPS* RNA (Figure 5F). *SPARCLE 275* directly interacted with PARP-1 (but not with Ku80) with nanomolar affinity (K_d, 13.7 ± 6.4 nM), but PARP-1 did not interact with *ELCRAPS* RNA. Thus, *SPARCLE* and PARP-1 bind tightly. Ku80 and DNA-PK$_{CS}$ may have been pulled down with *SPARCLE* in the RAP-MS proteome because they associate with PARP-1 in DDR complexes, but they are unlikely to directly interact strongly with *SPARCLE*.

SPARCLE deficiency enhances DNA-damage repair

Because *SPARCLE* interacts with PARP-1 and increases apoptosis after DNA damage, we hypothesized that *SPARCLE* interferes with DDR. To test this hypothesis, the extent of NCS-induced unrepaired DNA damage was compared in WT and *SPARCLE* KO HCT116 by counting γH2A.X foci that assemble at DSB using confocal microscopy (Figures 6A and 6B), and the percentage of cells with unrepaired DNA breaks marked with terminal deoxynucleotidyl transferase dUTP nick end labeling (TUNEL) by flow cytometry (Figure 6C). WT and *SPARCLE* KO cells both similarly increased γH2A.X foci for the first 36 h after adding NCS (Figure 6A). However, at 48 h, when *SPARCLE* is well expressed, *SPARCLE* KO cells had ~3-fold

(D) RAP-western blots (RAP-WB) probed for PARP-1 (left) or Ku80 (right) comparing input and *SPARCLE* pull-down (RAP) of nuclei of DOX-treated WT and *SPARCLE KO* HCT116.

(E) *SPARCLE* RNA immunoprecipitation (RIP). PARP-1 (left) or Ku80 (right) immunoprecipitates of nuclear lysates of untreated or DOX-treated WT and *SPARCLE* KO HCT116 amplified by qRT-PCR for *SPARCLE*. Cells lysed 48 h after adding DOX.

(F) Microscale thermophoresis (MST). Binding of Alexa 647-labeled PARP-1 (left) or Ku70/Ku80 (right) to *SPARCLE 275* or of Alexa 647-labeled PARP-1 (middle) to *ELCRAPS*.

Graphs show mean ± SEM of 3 technical replicates, and data are representative of at least 3 independent experiments; ***p < 0.001 by two-tailed t test; comparing WT and *SPARCLE* KO cells (E).

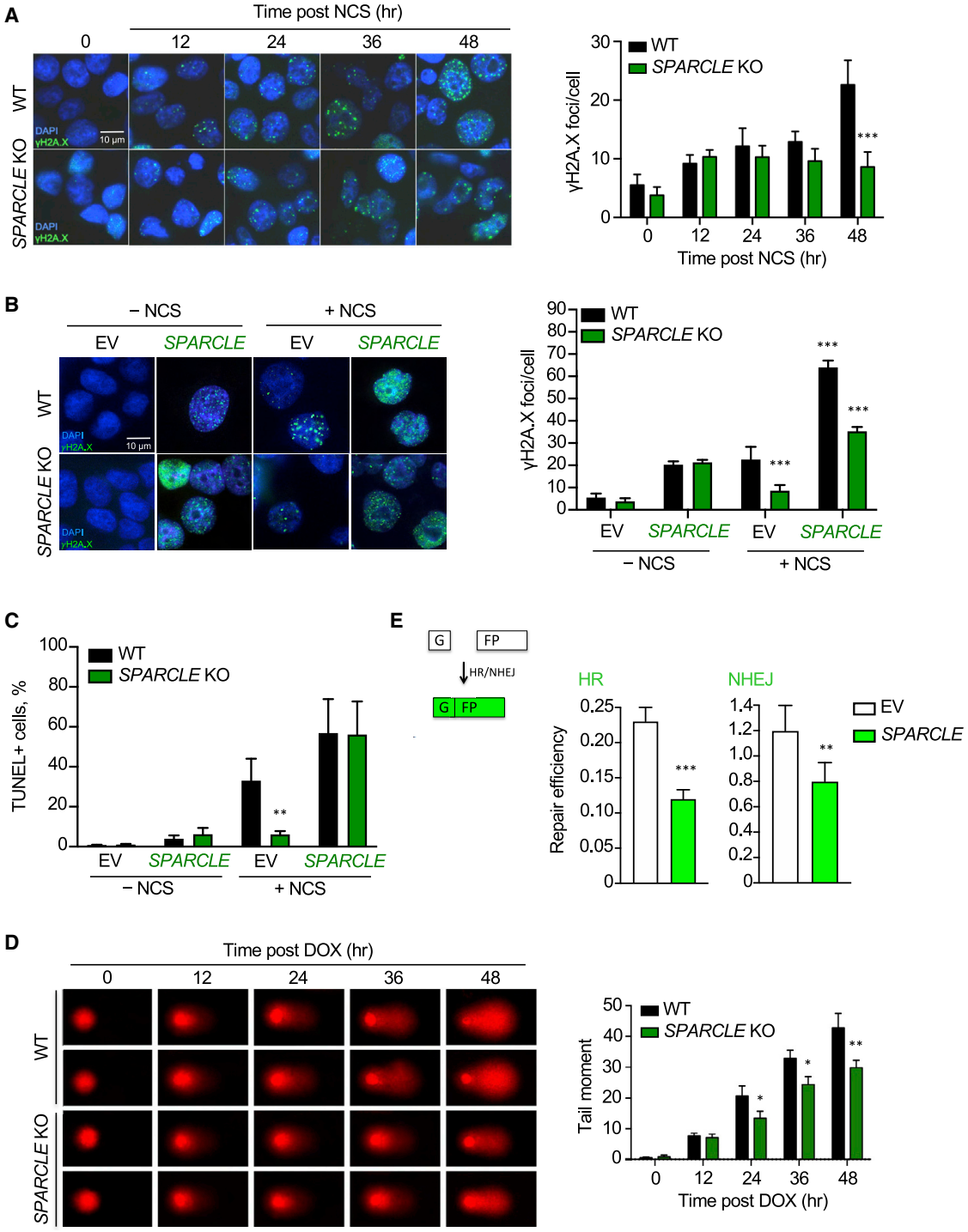

Figure 6. *SPARCLE* inhibits DNA repair

(A) γH2A.X foci (green) by immunofluorescence microscopy after NCS treatment of WT and *SPARCLE* KO HCT116. DAPI staining in blue. Shown are representative images (left) and the number of foci/cell in 3 independent experiments (right).

(B) γH2A.X foci (green) by immunofluorescence microscopy 48 h after adding NCS or medium to WT and *SPARCLE* KO HCT116 transfected with empty vector (EV) or an expression plasmid encoding the 5′ 275 nt of *SPARCLE* (*SPARCLE 275*). Shown are representative images (left) and image quantification of 3 experiments.

(C) TUNEL staining 48 h after adding medium or NCS to WT and *SPARCLE* KO HCT116 transfected 24 h earlier with EV or *SPARCLE 275*.

(legend continued on next page)

fewer γH2A.X foci. Similarly, 48 h after NCS treatment, virtually no *SPARCLE* KO cells were TUNEL+, while about a third of WT HCT116 had unrepaired TUNEL-stained DNA breaks. Ectopic expression of *SPARCLE 275* significantly increased the number of γH2A.X foci in NCS-treated WT HCT116 and significantly increased γH2A.X foci and TUNEL+ cells in *SPARCLE* KO cells, confirming that *SPARCLE* inhibits DNA repair, leaving more unrepaired DNA damage, and that the 5′ 275-nt fragment is the active region (Figures 6B and 6C). To confirm this finding, DNA damage was compared over 48 h in DOX-treated WT and *SPARCLE* KO HCT116 cells by COMET assay (single-cell gel electrophoresis) (Figure 6D). The comets in WT HCT116 cells contained more DNA tail fragments that migrated more rapidly to produce longer tails than in *SPARCLE* KO HCT116, leading to significantly larger COMET tail moments beginning at 24 h when *SPARCLE* is first detected.

To confirm that *SPARCLE 275* interferes with DSB repair and evaluate which DSB repair pathway it inhibits, a *SPARCLE 275* expression plasmid or empty vector (EV) was co-transfected in WT HCT116 with homologous recombination (HR) or NHEJ GFP reporter constructs that restore GFP fluorescence if they are repaired (Seluanov et al., 2010). Expression of *SPARCLE 275* significantly reduced HR by ∼50% and NHEJ by ∼35% (Figure 6E). Thus, *SPARCLE* reduced both HR- and NHEJ-mediated DNA repair.

SPARCLE enhances caspase-3-mediated cleavage of PARP-1

To understand how *SPARCLE* interaction with PARP-1 inhibits DDR, we first examined whether *SPARCLE* KO affects expression or cleavage of PARP-1 under basal conditions 24 and 48 h after inducing DSB by adding NCS to HCT116 or DOX to A549 and HepG2. PARP-1 cleavage is a hallmark of apoptosis (Figure 7A). Activated caspase-3 and caspase-7 cleave 116-kDa FL PARP-1 into 24-kDa NT and 89-kDa CT domains, inactivating PARP-1 by separating the NT DNA-binding domain from the automodification and catalytic domains (Chaitanya et al., 2010; D'Amours et al., 2001; Smulson et al., 1998). Without DNA damage, PARP-1 was expressed comparably in *SPARCLE* KO and WT cells, and cleaved PARP-1 was not detected (Figures 7B and S5A). After DNA damage, a PARP-1 immunoreactive band was detected of the size expected for NT-PARP1 after caspase cleavage. NT-PARP-1 was detected at 24 h but increased after 48 h, paralleling changes in *SPARCLE* expression. *SPARCLE* KO cells had no apparent change in FL PARP-1 compared with WT cells but significantly less cleaved NT-PARP-1, suggesting that *SPARCLE* promotes PARP-1 cleavage (Figures 7B and S5A). To confirm that *SPARCLE* increases PARP-1 cleavage, we ectopically expressed *SPARCLE 275* or EV in WT and *SPARCLE* KO HCT116 cells (Figure 7C). As in untransfected cells, NT-PARP-1 was significantly reduced in *SPARCLE* KO compared with WT cells after EV transfection. However, ectopic *SPARCLE 275* greatly increased NT-PARP-1 in both WT and *SPARCLE* KO HCT116. Similar results were obtained in WT and *SPARCLE KO* A549 and HepG2 cells transfected with *SPARCLE 275* but no increase in NT-PARP-1 was observed in cells that expressed *ELCRAPS* (Figure S5B). Thus, *SPARCLE* enhances PARP-1 cleavage. Reduced PARP-1 cleavage and apoptosis after DNA damage in *SPARCLE* KO cells could be caused by reduced caspase-3 activity. However, although p53 KO reduced caspase-3 activity 48 h after adding NCS, *SPARCLE* KO had no effect on activated caspase-3 (Figure S5C), indicating that *SPARCLE*'s effect on PARP-1 cleavage was not due to a change in caspase-3 activation.

To investigate whether enhanced PARP-1 cleavage was a direct or indirect effect, R-PARP-1 and active caspase-3 (R-caspase-3, recombinant caspase-3) (Figure S5D) were incubated for 10 min with *in vitro* transcribed *SPARCLE 275* or *ELCRAPS* (Figure S5E). Because cells express few copies of *SPARCLE*, to mimic cellular conditions *SPARCLE* was added at very low concentrations ranging from $1/100^{th}$ to $1/1{,}000^{th}$ the molar concentration of PARP-1. Even at the lowest concentration, *SPARCLE* dramatically enhanced PARP-1 cleavage, while *ELCRAPS* was inactive (Figure 7D). To determine whether the first 275 nt of *SPARCLE* were essential to enhance PARP-1 cleavage, we generated truncated *in vitro* transcribed RNA versions of *SPARCLE* encoding its first 75 nt (*SPARCLE 75*) or first 178 nt (*SPARCLE 178*) (Figure S5E). Although NT-PARP-1 was readily detected after a brief incubation of FL PARP-1 with *SPARCLE 275* and caspase-3, no cleaved PARP-1 was detected when *SPARCLE 75*, *SPARCLE 178*, or *ELCRAPS* substituted for *SPARCLE 275* or when caspase-3 was omitted (Figure 7E). Thus, most of the 5′-end of *SPARCLE 275* is needed to enhance caspase-3-mediated PARP-1 cleavage.

To investigate if PARP-1 catalytic activity is important for *SPARCLE* function, apoptosis was analyzed in cells treated with the PARP inhibitor Olaparib, added at the same time as NCS. PARP-1 inhibition did not restore apoptosis in *SPARCLE* KO or p53 KO HCT116 to WT levels (Figure S5F). These data suggest that the main mechanism by which *SPARCLE* increases apoptosis is by enhancing PARP-1 cleavage by caspase-3, rather than by directly altering its catalytic activity.

NT-PARP-1 interferes with DNA repair and restores DNA-damage-induced apoptosis in *SPARCLE* KO cells

Because caspase-3 separates the DNA-binding and catalytic domains of PARP-1, we hypothesized that NT-PARP-1 would bind to DNA breaks without recruiting DNA repair factors and thus block DNA repair. In support of this hypothesis, two studies showed that NT-PARP-1 binds to DNA breaks and decreases DSB repair *in vitro* (Smulson et al., 1998; Yung and Satoh, 2001). *SPARCLE*'s enhancement of PARP-1 cleavage to

(D) COMET assay by confocal microscopy of DOX-treated WT and *SPARCLE* KO HCT116. Shown are representative images (left) and quantified tail moments of 60 comets at each time point (right).

(E) Homologous recombination (HR, left) and non-homologous end joining (NHEJ, right) GFP reporter assays in WT HCT116 co-transfected with empty vector (EV) or *SPARCLE 275* and reporter plasmids. GFP analyzed by flow cytometry 72 h after transfection.

Graphs show mean ± SEM of 3 technical replicates (A–C and E). Data are representative of at least 3 independent experiments; *$p < 0.05$, **$p < 0.01$, ***$p < 0.001$ by two-tailed t test; comparing WT and *SPARCLE* KO cells (A–D) and EV and *SPARCLE* overexpressing cells (B and E).

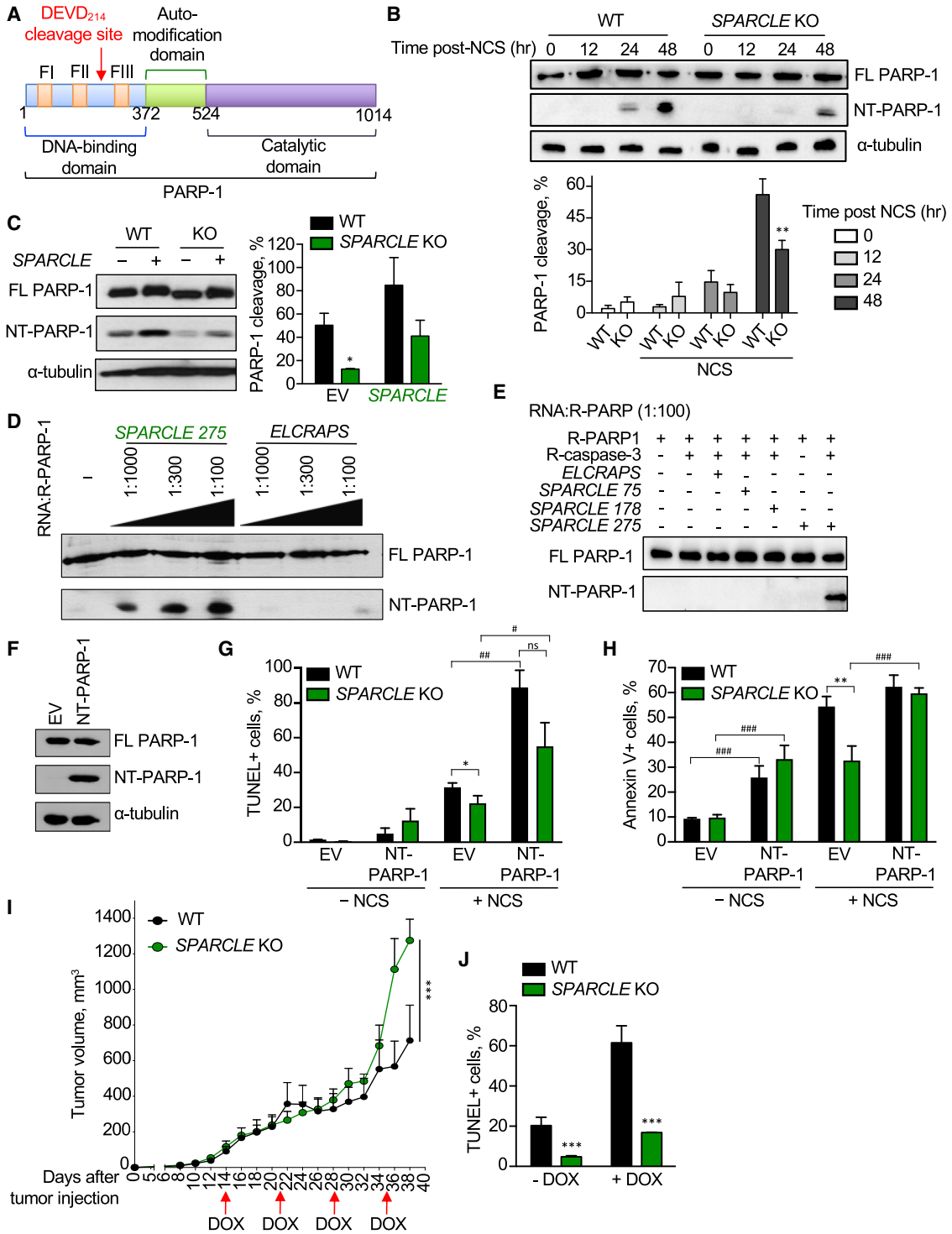

Figure 7. *SPARCLE* enhances caspase-3 cleavage of PARP-1 to inhibit DNA repair and increase apoptosis after DNA damage

(A) PARP-1 domains. FI-FIII are zinc-finger domains. Arrow shows the caspase-3/7 cleavage site.

(B) PARP-1 immunoblot of lysates from untreated and NCS-treated WT and *SPARCLE* KO HCT116. α-tubulin probed as loading control. Representative blot (top); densitometry quantification of 3 blots (bottom). FL, full-length; NT, N-terminal

(C) PARP-1 immunoblot of lysates from WT and *SPARCLE* KO HCT116 cells transfected with empty vector or *SPARCLE 275*. α-tubulin probed as loading control. Representative blot (top); densitometry quantification of 3 blots (bottom).

(legend continued on next page)

generate more NT-PARP-1 would then lead to more unrepaired DNA damage and thereby increase apoptosis. To test this hypothesis, the effect of NT-PARP-1 ectopic expression on DNA repair and apoptosis in WT and *SPARCLE* KO cells was analyzed (Figures 7F–7H). Modest PARP-1-NT OE, which did not alter FL PARP-1 levels (Figure 7F), increased TUNEL (Figure 7G) and annexin V (Figure 7H) staining similarly in WT and *SPARCLE* KO cells under basal conditions suggesting that NT-PARP-1 interfered with repair of endogenous DNA damage, such as occurs during DNA replication. As expected, NCS treatment of EV-transfected cells led to significantly less TUNEL staining and apoptosis in *SPARCLE* KO than WT cells. However, these differences became insignificant in cells transfected to express NT-PARP-1. Because NT-PARP-1 expression rescues *SPARCLE* deficiency, the main mechanism by which *SPARCLE* inhibits DNA repair and increases apoptosis is likely by enhancing caspase-3 cleavage of PARP-1.

SPARCLE KO tumors are relatively resistant to chemotherapy

Our model suggests that *SPARCLE* KO cells will be relatively resistant to DNA damage because they more efficiently repair damage and are less likely to undergo apoptosis. To test *SPARCLE*'s *in vivo* importance, WT or *SPARCLE* KO HCT116 (3×10^6 cells/mouse) were implanted subcutaneously into nude mice (10 mice/group) and 2 weeks later, when tumors were clearly palpable, mice were treated weekly intraperitoneally with DOX (Figure 7I). *SPARCLE* KO had no significant effect on tumor size before chemotherapy or for the first 3 weeks of chemotherapy, suggesting that *SPARCLE* expression did not affect tumor cell proliferation or survival in the absence of therapy. However, after 3 weeks of treatment, *SPARCLE* KO tumors became significantly larger. Because of tumor size, mice had to be sacrificed 40 days after implantation and 4 days after the fourth DOX dose. At sacrifice, *SPARCLE* KO HCT116 xenografts had reduced TUNEL staining compared with WT xenografts (Figure 7J). Thus, *SPARCLE* inhibits DNA repair and promotes apoptosis after DNA damage *in vivo* and its absence modestly, but significantly, promotes HCT116 tumor growth.

DISCUSSION

Here, we identify *SPARCLE*, a p53-induced nuclear lncRNA expressed only at low copy number at late stages of apoptosis, as a profound mediator of cell death after DNA damage. *SPARCLE* potently interferes with DNA repair in *trans* by promoting PARP-1 cleavage by caspase-3. When *SPARCLE* is genetically inactivated, DNA-damaged cells fail to undergo p53-mediated apoptosis. This anti-apoptotic phenotype is rescued by OE NT-PARP-1, indicating that promoting PARP-1 cleavage is *SPARCLE*'s main mode of action. PARP-1 cleavage is a hallmark of apoptosis. PARP-1 acts at an early stage of DNA damage to sense DNA breaks and recruit the DNA repair machinery. PARP-1 cleavage helps maintain ATP levels, which would otherwise become depleted secondary to NAD^+ depletion during PARylation. Cells need ATP to undergo apoptosis rather than die by necrosis (Gibson and Kraus, 2012; Li and Yu, 2015; Schreiber et al., 2006). However, the potent pro-apoptotic effect of NT-PARP-1 in the setting of DNA damage, which we demonstrate here, has not been fully appreciated (Wang et al., 2018). Our model is that cleaved NT-PARP-1 binds to DNA, but because it lacks the other PARP-1 domains, fails to recruit DNA repair factors to DNA breaks and consequently blocks DNA damage repair, as has been previously suggested (D'Amours et al., 2001; Smulson et al., 1998). Unrepaired DNA breaks then trigger apoptosis. *SPARCLE* reduces p53-mediated apoptosis and increases G1 arrest. Because *SPARCLE* only begins to be expressed 1 day after DNA damage is triggered, we speculate that *SPARCLE*'s role is to guarantee that cells with extensive DNA damage that has not been completely repaired 1 or 2 days later die, since they may carry deleterious mutations that could interfere with normal cellular functions or promote tumor formation.

SPARCLE is not expressed in the absence of DNA damage and is expressed at such low levels and so late after DNA damage that it has not been clearly annotated in the transcriptome. It also was not identified as a p53-induced lncRNA in studies that screened for p53-induced ncRNAs and uncovered p53-regulated lncRNAs including *lincRNA-p21* (Huarte et al., 2010), *TP53TG1* (Diaz-Lagares et al., 2016), *MEG3* (Zhu et al., 2015), *Neat1* (Adriaens et al., 2016), *DDSR1* (Sharma et al., 2015), *DINO* (Schmitt et al., 2016), *LINP1* (Zhang et al., 2016), *PURPL* (Li et al., 2017), *PINCR* (Chaudhary et al., 2017), and *GUARDIN* (Hu et al., 2018).

It is surprising that a poorly expressed lncRNA so potently affects cell death. However, the mechanism of action for *SPARCLE* acting as a cofactor for caspase-3 cleavage of PARP-1 is strongly supported by the *in vitro* cleavage experiment with purified active caspase-3 and PARP-1 and *in vitro* transcribed *SPARCLE*. Addition of *SPARCLE* at only one thousandth the molar ratio of PARP-1 unambiguously promoted PARP-1 cleavage. Our model is that *SPARCLE* acts as a scaffold

(D and E) Effect of adding *SPARCLE 275* or *ELCRAPS* (D) or *SPARCLE 75*, *SPARCLE 178*, *SPARCLE 275*, or *ELCRAPS* RNA (E) on *in vitro* recombinant caspase-3 (R-caspase-3)-mediated cleavage of recombinant PARP-1 (R-PARP-1), analyzed by immunoblot. RNA:PARP-1 molar ratios indicated. Representative blot of 3 replicates.

(F–H) Effect of overexpression of NT-PARP-1, compared with empty vector (EV), in WT HCT116 on NCS-induced DNA damage (TUNEL staining by flow cytometry, G) and cell death (annexin V+ by flow cytometry, H) assessed after 48 h. (F) Immunoblot of untreated WT HCT116 lysates probed for FL- (endogenous) and NT- (exogenous) PARP-1 or loading control.

(I) WT or *SPARCLE* KO HCT116 xenograft tumor size in nude mice (n = 10/group) treated weekly after tumors became palpable with intraperitoneal DOX. Mice sacrificed 40 days after implantation.

(J) TUNEL staining of tumor sections obtained at sacrifice, quantified in at least 3 microscopic fields.

(B, C, G, H, and J) graphs show mean ± SEM of 3 technical replicates and data are representative of at least 3 independent experiments; two-tailed t tests compare WT with *SPARCLE* KO $^*p < 0.05$, $^{**}p < 0.01$, $^{***}p < 0.001$ (B, C, G, H, and J) and compare EV with NT-PARP-1 transfection $^{\#}p < 0.05$, $^{\#\#}p < 0.01$, $^{\#\#\#}p < 0.001$ (G and H). (I) Analyzed by one-way ANOVA using the Holm-Sidak method. $^{***}p < 0.001$.

to bring PARP-1 and caspase-3 together and promote its cleavage. Cells are estimated to contain ~2 × 10^5 PARP-1 molecules/cell (Liu et al., 2017). Our data suggest that *SPARCLE* is about ten thousand times less abundant after DNA damage (~8–16 copies/cell) than PARP-1. Thus, the 1:1,000 *SPARCLE*:PARP-1 molar ratio used in our *in vitro* cleavage experiment may come close to the physiological ratio. The strong nanomolar affinity we measured for the PARP-1:*SPARCLE* interaction may be important for its potent biological effect despite its low expression. Although *SPARCLE* binds to both FL and NT-PARP-1, our model is that once cleaved, NT-PARP-1 detaches allowing another FL molecule to bind. We are unaware of any previous example of a lncRNA acting as a protease cofactor.

lncRNAs have previously been shown to act as protein scaffolds (Chu et al., 2011). However, most of the examples of lncRNA scaffolds involve assembling protein complexes on chromatin (examples are the telomerase RNA *TERC* and *HOTAIR* and *ANRIL* that interact with polycomb repressor complexes) or on RNA that take advantage of sequence complementarity to enhance binding. However, lncRNAs can also bind to proteins independently of interactions with other nucleic acids. One lncRNA example is *NKILA* the cytoplasmic lncRNA that binds to the NF-κB/IκB complex and stabilizes it by masking IκB phosphorylation sites (Huang et al., 2018).

After DSB induction, *SPARCLE*-deficient miR-34b/c KO, p53RE2 KO, and *SPARCLE* KO HCT116 arrested in G1, while p53 KO HCT116 arrested at G2/M (Figures 1G, 3C, and 4D). p53 activation can cause both G1 and G2/M arrest, which it does by regulating many genes. One of the most important p53 induced genes is *CDKN1A* which encodes for p21, which inhibits CDK4/6 that plays an important role in progression from G1. *SPARCLE* mostly affects cell death by interfering with DNA repair. Unrepaired DSBs in *SPARCLE* sufficient cells are expected to trigger the ATR response and activate CHK1 to cause G2/M arrest. However, in the absence of *SPARCLE*, this checkpoint would not be as strongly induced, but other p53-induced checkpoints could become more prominent. p53-induced genes other than *SPARCLE*, such as *CDKN1A*, are likely responsible for the difference in cell-cycle arrest between p53 KO cells and miR-34b/c KO, p53RE2 KO, and *SPARCLE* KO cells.

The PARP-1 cleavage promoting activity of the ~770 nt lncRNA was contained within its 5′ 275 nt sequence and required more than the first 178 5′ sequence. Even though we found that the first 275 nt are critical for PARP-1 cleavage, it is possible that the rest of the lncRNA may also have a functional role. Future work will need to identify the critical residues and two-dimensional and three-dimensional structures important for *SPARCLE* binding and function. Although a few *SPARCLE* SNPs have been reported, it is unknown whether they have functional consequences or might be linked to diseases such as cancer. Based on the strong pro-apoptotic effect of *SPARCLE* post-DNA damage, one might expect that *SPARCLE* expression might be suppressed by mutation or promoter methylation in p53-sufficient cancers or that *SPARCLE* suppression might occur in chemotherapy or irradiated tumors as a mechanism of resistance. It will be worthwhile to look for a link between *SPARCLE* and prognosis and drug resistance of p53-sufficient tumors. It is also possible that *SPARCLE* has other activities, such as in splicing, based on the candidate RAP-MS-interacting proteins, which we did not investigate. Future studies could investigate some of the other potential *SPARCLE*-interacting proteins that were detected in the *SPARCLE* pull-down, which we did not pursue in this study.

The expression of the miR-34b/c cluster and *SPARCLE* are closely linked. They both use the same p53RE in their promoter and may even be expressed in the same primary transcript. The primary transcript of the miR-34b/c cluster has not been defined. Since deletion of miR-34b and miR-34c also reduced *SPARCLE* expression (Figure 2A), but the converse was not true (deletion of 253 nt of *SPARCLE* did not delete mature miR-34b or miR-34c) (Figures 4B, S3A, and S3B), one intriguing possibility is that *SPARCLE* and these miRNAs are transcribed on the same pri-miRNA transcript that is processed by DROSHA into *SPARCLE* (or a longer precursor) and a pre-miRNA encoding miR-34b and miR-34c. Such a model would explain its low copy number and the fact that *SPARCLE* is 5′-capped but likely does not have a poly(A) tail. Processing of a shared primary transcript or the stability of each of its products might be regulated after genotoxic damage since miR-34b/c are both similarly expressed at 24 and 48 h, while *SPARCLE* expression greatly increases between 24 and 48 h (Figures 2A and S1A). However, additional work is needed to define the biogenesis of *SPARCLE* and its potential link to miR-34b/c.

Limitations of the study

SPARCLE's low copy number makes it challenging to study. For example, attempts to use smFISH to colocalize *SPARCLE* with other factors (for example with PARP-1 or DNA repair foci) were unsuccessful. Therefore, we were unable to verify that *SPARCLE* reduced the recruitment of DNA repair factors to DNA-damage sites. Although *SPARCLE* localized mostly to the nucleus, we do not know if *SPARCLE* catalyzes PARP-1 cleavage by caspase-3 (which has been found in the nucleus [Kamada et al., 2005; Luo et al., 2010]) when PARP-1 is bound to DNA breaks or in solution. Structural studies of *SPARCLE* interacting with PARP-1 and caspase-3 could lead to a better understanding of *SPARCLE*'s role in promoting caspase-3 cleavage of PARP-1. The formation of a stable complex might require using a catalytically dead mutant of caspase-3 or RNase-resistant *SPARCLE*. The *SPARCLE* primary transcript remains to be defined. One attractive hypothesis that could be explored using *Drosha* and/or *Dicer* KO cell lines is that *SPARCLE* and mir-34b/c are transcribed as one transcript that is processed by the RNAi machinery.

STAR★METHODS

Detailed methods are provided in the online version of this paper and include the following:

- KEY RESOURCES TABLE
- RESOURCE AVAILABILITY
  - Lead contact
  - Materials availability
  - Data and code availability

- EXPERIMENTAL MODEL AND SUBJECT DETAILS
  - Cell lines and culture conditions
  - Animal experiments
- METHOD DETAILS
  - Cell treatments
  - RNA extraction
  - qRT-PCR
  - Cell cycle analysis
  - Annexin V staining
  - miRNA mimics and plasmid transfection
  - Gene knockdown
  - 5' and 3' rapid amplification of cDNA ends (RACE)
  - Circular RACE (cRACE)
  - Luciferase assays
  - Chromatin immunoprecipitation (ChIP)
  - *SPARCLE* Taqman qPCR
  - Cell fractionation
  - Immunoblot
  - Single-molecule FISH (smFISH)
  - *SPARCLE* truncations
  - PARP-1 N-terminal domain (PARP-1-NT) cloning
  - Generation of miR-34b/c KO and p53RE2 KO HCT116 cells using TALENs
  - Generation of *SPARCLE* KO HCT116, A549 and HepG2 cells using CRISPR/Cas9
  - RNA-seq libraries and sequencing
  - RNA antisense purification-mass spectrometry (RAP-MS)
  - RNA immunoprecipitation (RIP)
  - TUNEL assay
  - COMET assay
  - HR and NHEJ reporter assays
  - Immunofluorescence
  - *In vitro* transcription
  - PARP-1 *in vitro* cleavage
  - Microscale thermophoresis (MST)
  - PARP-1 inhibition
  - Caspase-3 activity assay
  - TUNEL immunohistochemistry
- QUANTIFICATION AND STATISTICAL ANALYSIS
  - Quantification
  - Statistics
  - RNA-seq analysis

SUPPLEMENTAL INFORMATION

Supplemental information can be found online at https://doi.org/10.1016/j.molcel.2022.01.001.

ACKNOWLEDGMENTS

We thank Dipanjan Chowdhury (Dana Farber Cancer Institute) for NHEJ antibodies, Vera Gorbunova (University of Rochester) for DSB repair reporter plasmids, David Valle-Garcia (National University of Mexico) for bioinformatic advice, and Jonathan Salazar-León (National University of Mexico) for assistance with the graphical abstract using BioRender. This work was supported by NIH R01DA039566 (J.L.), Pew Latin American Fellowship in the Biomedical Sciences and Mexican National Council of Science and Technology (CONACyT) Postdoctoral Fellowship (CVU: 331537) (K.F.M.-S.), Glaxo Smith Kline-Immune Disease Institute Alliance Fellowship (F.N.), CRI Irvington Postdoctoral Fellowship (R.M.), US Department of Defense Breast Cancer Breakthrough Fellowship (Y.Z.), DGAPA-PAPIIT IN213119 (L.P.-M.) and IN211719 (G.P.-A.) Intramural Research Program of the National Cancer Institute (NCI), Center for Cancer Research (CCR), NIH (A.L.), and CONACyT grant IFC 2016-2282 (L.P.-M). K.F.M.-S. is member of the Mexican National System of Researchers (SNI).

AUTHOR CONTRIBUTIONS

Conceptualization, K.F.M.-S., F.N., and J.L.; methodology, K.F.M.-S. and F.N.; validation, K.F.M.-S.; formal analysis, K.F.M.-S.; investigation, K.F.M.-S., R.M., F.N., Z.Z., Y.Z., C.C.R.H., X.L.L., and J.J.H.; resources and supervision, G.P.-A., L.P.-M., A.L., H.W., and J.L.; writing – original draft, K.F.M.-S. and J.L.; writing – review & editing, all authors; funding acquisition, J.L.

DECLARATION OF INTERESTS

The authors declare no competing interests.

Received: February 5, 2020
Revised: January 4, 2022
Accepted: January 4, 2022
Published: January 31, 2022

REFERENCES

Adriaens, C., Standaert, L., Barra, J., Latil, M., Verfaillie, A., Kalev, P., Boeckx, B., Wijnhoven, P.W., Radaelli, E., Vermi, W., et al. (2016). p53 induces formation of NEAT1 lncRNA-containing paraspeckles that modulate replication stress response and chemosensitivity. Nat. Med. *22*, 861–868.

Beck, C., Robert, I., Reina-San-Martin, B., Schreiber, V., and Dantzer, F. (2014). Poly(ADP-ribose) polymerases in double-strand break repair: focus on PARP1, PARP2 and PARP3. Exp. Cell Res. *329*, 18–25.

Bieging-Rolett, K.T., Kaiser, A.M., Morgens, D.W., Boutelle, A.M., Seoane, J.A., Van Nostrand, E.L., Zhu, C., Houlihan, S.L., Mello, S.S., Yee, B.A., et al. (2020). Zmat3 is a key splicing regulator in the p53 tumor suppression program. Mol. Cell *80*, 452–469.

Bunz, F., Hwang, P.M., Torrance, C., Waldman, T., Zhang, Y., Dillehay, L., Williams, J., Lengauer, C., Kinzler, K.W., and Vogelstein, B. (1999). Disruption of p53 in human cancer cells alters the responses to therapeutic agents. J. Clin. Invest. *104*, 263–269.

Ceccaldi, R., Rondinelli, B., and D'Andrea, A.D. (2016). Repair pathway choices and consequences at the double-strand break. Trends Cell Biol *26*, 52–64.

Chaitanya, G., Alexander, J.S., and Babu, P. (2010). PARP-1 cleavage fragments: signatures of cell-death proteases in neurodegeneration. Cell Commun. Signal. *8*, 5–11.

Chang, H.H.Y., Pannunzio, N.R., Adachi, N., and Lieber, M.R. (2017). Non-homologous DNA end joining and alternative pathways to double-strand break repair. Nat. Rev. Mol. Cell Biol. *18*, 495–506.

Chaudhary, R., Gryder, B., Woods, W.S., Subramanian, M., Jones, M.F., Li, X.L., Jenkins, L.M., Shabalina, S.A., Mo, M., Dasso, M., et al. (2017). Prosurvival long noncoding RNA PINCR regulates a subset of p53 targets in human colorectal cancer cells by binding to Matrin 3. Elife *6*, 1–32.

Chaudhary, R., and Lal, A. (2017). Long noncoding RNAs in the p53 network. Wiley Interdiscip. Rev. RNA *8*, 1–17.

Chu, C., Qu, K., Zhong, F.L., Artandi, S.E., and Chang, H.Y. (2011). Genomic maps of long noncoding RNA occupancy reveal principles of RNA-chromatin interactions. Mol. Cell *44*, 667–678.

Concepcion, C.P., Han, Y.C., Mu, P., Bonetti, C., Yao, E., D'Andrea, A., Vidigal, J.A., Maughan, W.P., Ogrodowski, P., and Ventura, A. (2012). Intact p53-dependent responses in miR-34-deficient mice. PLoS Genet *8*, e1002797.

D'Amours, D., Sallmann, F.R., Dixit, V.M., and Poirier, G.G. (2001). Gain-of-function of poly(ADP-ribose) polymerase-1 upon cleavage by apoptotic proteases: implications for apoptosis. J. Cell Sci. *114*, 3771–3778.

Dangelmaier, E., Lazar, S.B., and Lal, A. (2019). Long noncoding RNAs: p53's secret weapon in the fight against cancer? PLoS Biol *17*, e3000143.

Diaz-Lagares, A., Crujeiras, A.B., Lopez-Serra, P., Soler, M., Setien, F., Goyal, A., Sandoval, J., Hashimoto, Y., Martinez-Cardús, A., Gomez, A., et al. (2016). Epigenetic inactivation of the p53-induced long noncoding RNA TP53 target 1 in human cancer. Proc. Natl. Acad. Sci. USA *113*, E7535–E7544.

Engreitz, J.M., Pandya-Jones, A., McDonel, P., Shishkin, A., Sirokman, K., Surka, C., Kadri, S., Xing, J., Goren, A., Lander, E.S., et al. (2013). The Xist lncRNA exploits three-dimensional genome architecture to spread across the X chromosome. Science *341*, 1237973.

Gibson, B.A., and Kraus, W.L. (2012). New insights into the molecular and cellular functions of poly(ADP-ribose) and PARPs. Nat. Rev. Mol. Cell Biol. *13*, 411–424.

Grossi, E., Sánchez, Y., and Huarte, M. (2016). Expanding the p53 regulatory network: LncRNAs take up the challenge. Biochim. Biophys. Acta *1859*, 200–208.

Halappanavar, S.S., Le Rhun, Y.L., Mounir, S., Martins, L.M., Huot, J., Earnshaw, W.C., and Shah, G.M. (1999). Survival and proliferation of cells expressing caspase-uncleavable poly(ADP-ribose) polymerase in response to death-inducing DNA damage by an alkylating agent. J. Biol. Chem. *274*, 37097–37104.

He, L., He, X., Lim, L.P., Stanchina, E., De Xuan, Z., Liang, Y., Xue, W., Zender, L., Magnus, J., Ridzon, D., et al. (2007). A microRNA component of the p53 tumour suppressor network. Nature *447*, 1130–1134.

Hermeking, H. (2007). p53 enters the microRNA world. Cancer Cell *12*, 414–418.

Hu, W.L., Jin, L., Xu, A., Wang, Y.F., Thorne, R.F., Zhang, X.D., and Wu, M. (2018). *GUARDIN* is a p53-responsive long non-coding RNA that is essential for genomic stability. Nat. Cell Biol. *20*, 492–502.

Huang, D., Chen, J., Yang, L., Ouyang, Q., Li, J., Lao, L., Zhao, J., Liu, J., Lu, Y., Xing, Y., et al. (2018). NKILA lncRNA promotes tumor immune evasion by sensitizing T cells to activation-induced cell death. Nat. Immunol. *19*, 1112–1125.

Huarte, M. (2015). The emerging role of lncRNAs in cancer. Nat. Med. *21*, 1253–1261.

Huarte, M., Guttman, M., Feldser, D., Garber, M., Koziol, M.J., Kenzelmann-Broz, D., Khalil, A.M., Zuk, O., Amit, I., Rabani, M., et al. (2010). A large intergenic noncoding RNA induced by p53 mediates global gene repression in the p53 response. Cell *142*, 409–419.

Kamada, S., Kikkawa, U., Tsujimoto, Y., and Hunter, T. (2005). Nuclear translocation of caspase-3 is dependent on its proteolytic activation and recognition of a substrate-like protein(s). J. Biol. Chem. *280*, 857–860.

Kang, Y.J., Yang, D.C., Kong, L., Hou, M., Meng, Y.Q., Wei, L., and Gao, G. (2017). CPC2: a fast and accurate coding potential calculator based on sequence intrinsic features. Nucleic Acids Res *45*, W12–W16.

Kastenhuber, E.R., and Lowe, S.W. (2017). Putting p53 in context. Cell *170*, 1062–1078.

Lane, D.P. (1992). The guardian of the genome: p53. Nature *358*, 15–16.

Léveillé, N., Melo, C.A., Rooijers, K., Díaz-Lagares, A., Melo, S.A., Korkmaz, G., Lopes, R., Moqadam, F.A., Maia, A.R., Wijchers, P.J., et al. (2015). Genome-wide profiling of p53-regulated enhancer RNAs uncovers a subset of enhancers controlled by a lncRNA. Nat. Commun. *6*, 6520.

Li, J., and Xu, X. (2016). DNA double-strand break repair: a tale of pathway choices. Acta Biochim. Biophys. Sin. (Shanghai) *48*, 641–646.

Li, M., and Yu, X. (2015). The role of poly(ADP-ribosyl)ation in DNA damage response and cancer chemotherapy. Oncogene *34*, 3349–3356.

Li, X.L., Subramanian, M., Jones, M.F., Chaudhary, R., Singh, D.K., Zong, X., Gryder, B., Sindri, S., Mo, M., Schetter, A., et al. (2017). Long noncoding RNA PURPL suppresses basal p53 levels and promotes tumorigenicity in colorectal Cancer. Cell Rep *20*, 2408–2423.

Liao, Y., Smyth, G.K., and Shi, W. (2013). The Subread aligner: fast, accurate and scalable read mapping by seed-and-vote. Nucleic Acids Res *41*, e108.

Liu, L., Kong, M., Gassman, N.R., Freudenthal, B.D., Prasad, R., Zhen, S., Watkins, S.C., Wilson, S.H., and Van Houten, B. (2017). PARP1 changes from three-dimensional DNA damage searching to one-dimensional diffusion after auto-PARylation or in the presence of APE1. Nucleic Acids Res *45*, 12834–12847.

Luo, M., Lu, Z., Sun, H., Yuan, K., Zhang, Q., Meng, S., Wang, F., Guo, H., Ju, X., Liu, Y., et al. (2010). Nuclear entry of active caspase-3 is facilitated by its p3-recognition-based specific cleavage activity. Cell Res *20*, 211–222.

McCarthy, D.J., Chen, Y., and Smyth, G.K. (2012). Differential expression analysis of multifactor RNA-seq experiments with respect to biological variation. Nucleic Acids Res *40*, 4288–4297.

McHugh, C.A., Surka, C.F., Moradian, A., Hess, S., and Guttman, M. (2015). The Xist lncRNA interacts directly with SHARP to silence transcription through HDAC3. Nature *521*, 232–236.

Navarro, F., and Lieberman, J. (2015). miR-34 and p53: new insights into a complex functional relationship. PLoS One *10*, e0132767.

Oliver, F.J., De La Rubia, G., Rolli, V., Ruiz-Ruiz, M.C., De Murcia, G., and Murcia, J.M. (1998). Importance of poly(ADP-ribose) polymerase and its cleavage in apoptosis: lesson from an uncleavable mutant. J. Biol. Chem. *273*, 33533–33539.

Orjalo, A., Johansson, H.E., and Ruth, J.L. (2011). Stellaris fluorescence *in situ* hybridization (FISH) probes: a powerful tool for mRNA detection. Nat. Methods *8*, i, –ii.

Raj, A., van den Bogaard, P., Rifkin, S.A., van Oudenaarden, A., and Tyagi, S. (2008). Imaging individual mRNA molecules using multiple singly labeled probes. Nat. Methods *5*, 877–879.

Ramírez, F., Ryan, D.P., Grüning, B., Bhardwaj, V., Kilpert, F., Richter, A.S., Heyne, S., Dündar, F., and Manke, T. (2016). deepTools2: a next generation web server for deep-sequencing data analysis. Nucleic Acids Res *44*, W160–W165.

Raver-Shapira, N., Marciano, E., Meiri, E., Spector, Y., Rosenfeld, N., Moskovits, N., Bentwich, Z., and Oren, M. (2007). Transcriptional activation of miR-34a contributes to p53-mediated apoptosis. Mol. Cell *26*, 731–743.

Rokavec, M., Öner, M.G., Li, H., Jackstadt, R., Jiang, L., Lodygin, D., Kaller, M., Horst, D., Ziegler, P.K., Schwitalla, S., et al. (2014). IL-6R/STAT3/miR-34a feedback loop promotes EMT-mediated colorectal cancer invasion and metastasis. J. Clin. Invest. *124*, 1853–1867.

Sánchez, Y., Segura, V., Marín-Béjar, O., Athie, A., Marchese, F.P., González, J., Bujanda, L., Guo, S., Matheu, A., and Huarte, M. (2014). Genome-wide analysis of the human p53 transcriptional network unveils a lncRNA tumour suppressor signature. Nat. Commun. *5*, 5812.

Schmitt, A.M., Garcia, J.T., Hung, T., Flynn, R.A., Shen, Y., Qu, K., Payumo, A.Y., Peres-Da-Silva, A., Broz, D.K., Baum, R., et al. (2016). An inducible long noncoding RNA amplifies DNA damage signaling. Nat. Genet. *48*, 1370–1376.

Schreiber, V., Dantzer, F., Ame, J.C., and De Murcia, G. (2006). Poly(ADP-ribose): novel functions for an old molecule. Nat. Rev. Mol. Cell Biol. *7*, 517–528.

Seluanov, A., Mao, Z., and Gorbunova, V. (2010). Analysis of DNA double-strand break (DSB) repair in mammalian cells. J. Vis. Exp. (43) https://doi.org/10.3791/2002.

Sharma, V., Khurana, S., Kubben, N., Abdelmohsen, K., Oberdoerffer, P., Gorospe, M., and Misteli, T. (2015). A BRCA 1-interacting lncRNA regulates homologous recombination. EMBO Rep *16*, 1520–1534.

Smulson, M.E., Pang, D., Jung, M., Dimtchev, A., Chasovskikh, S., Spoonde, A., Simbulan-Rosenthal, C., Rosenthal, D., Yakovlev, A., and Dritschilo, A. (1998). Irreversible binding of poly(ADP)ribose polymerase cleavage product to DNA ends revealed by atomic force microscopy: possible role in apoptosis. Cancer Res *58*, 3495–3498.

Song, R., Walentek, P., Sponer, N., Klimke, A., Lee, J.S., Dixon, G., Harland, R., Wan, Y., Lishko, P., Lize, M., et al. (2014). miR-34/449 miRNAs are required for motile ciliogenesis by repressing cp110. Nature *510*, 115–120.

Spagnolo, L., Barbeau, J., Curtin, N.J., Morris, E.P., and Pearl, L.H. (2012). Visualization of a DNA-PK/PARP1 complex. Nucleic Acids Res *40*, 4168–4177.

Ting, N.S.Y., Kao, P.N., Chan, D.W., Lintott, L.G., and Lees-Miller, S.P. (1998). DNA-dependent protein kinase interacts with antigen receptor response element binding proteins NF90 and NF45. J. Biol. Chem. *273*, 2136–2145.

Ulitsky, I., and Bartel, D.P. (2013). *lincRNAs*: genomics, evolution, and mechanisms. Cell *154*, 26–46.

Vogelstein, B., Lane, D., and Levine, A.J. (2000). Surfing the p53 network. Nature *408*, 307–310.

Wang, O., Huang, Y., Wu, H., Zheng, B., Lin, J., and Jin, P. (2018). LncRNA LOC728196/miR-513c axis facilitates glioma carcinogenesis by targeting TCF7. Gene *679*, 119–125.

Wei, H., and Yu, X. (2016). Functions of PARylation in DNA damage repair pathways. Genomics Proteomics Bioinformatics *14*, 131–139.

Yung, T.M.C., and Satoh, M.S. (2001). Functional competition between poly(ADP-ribose) polymerase and its 24-kDa apoptotic fragment in DNA repair and transcription. J. Biol. Chem. *276*, 11279–11286.

Zhang, Y., He, Q., Hu, Z., Feng, Y., Fan, L., Tang, Z., Yuan, J., Shan, W., Li, C., Hu, X., et al. (2016). Long noncoding RNA LINP1 regulates repair of DNA double-strand breaks in triple-negative breast cancer. Nat. Struct. Mol. Biol. *23*, 522–530.

Zhu, J., Liu, S., Ye, F., Shen, Y., Tie, Y., Zhu, J., Wei, L., Jin, Y., Fu, H., Wu, Y., et al. (2015). Long noncoding RNA MEG3 interacts with p53 protein and regulates partial p53 target genes in hepatoma cells. PLoS One *10*, e0139790.

STAR★METHODS

KEY RESOURCES TABLE

REAGENT OR RESOURCE	SOURCE	IDENTIFIER
Antibodies		
Annexin V AlexaFluor647-conjugated antibody	ThermoFisher Scientific	Cat# A23204
Goat anti-rabbit IgG (H+L) highly cross-adsorbed Alexa Fluor 488 secondary antibody	ThermoFisher Scientific	Cat# A11034; RRID: AB_2576217
Mouse IgG2b, kappa monoclonal - Isotype Control	Abcam	Cat# ab170192
Mouse monoclonal anti-alpha-tubulin	Sigma-Aldrich	Cat# T5168; RRID: AB_477579
Mouse monoclonal anti-beta-actin	Developmental Studies Hybridoma Bank	Cat# JLA20-c; RRID: AB_528068
Mouse monoclonal anti-caspase-3	Abcam	Cat# [ABM1C12] (ab208161)
Mouse monoclonal anti-Ku86 (B-1)	Santa Cruz Biotechnology	Cat# sc-5280; RRID: AB_672929
Mouse monoclonal anti-Lamin A/C (E-1)	Santa Cruz Biotechnology	Cat# sc-376248; RRID: AB_10991536
Mouse monoclonal anti-p53 (DO-1)	Santa Cruz Biotechnology	Cat# sc-126; RRID: AB_628082
Mouse monoclonal anti-PARP1 (B-10)	Santa Cruz Biotechnology	Cat# sc-74470; RRID: AB_1127036
Rabbit monoclonal anti-Phospho-histone H2A.X (Ser139) (20E3)	Cell Signaling Technology	Cat# 9718S; RRID: AB_2118009
Bacterial and virus strains		
MAX efficiency DH5α competent cells	ThermoFisher Scientific	Cat# 18258012
Chemicals, peptides and recombinant proteins		
10X Annexin V Binding Buffer	BD Biosciences	Cat# 556454
Advanced Dulbecco's modified Eagle's medium (DMEM)	ThermoFisher Scientific	Cat# 12491-015
AmpliTaq DNA polymerase with Buffer I	Applied Biosystems	Cat# N8080166
AZD2461 (Olaparib analog)	Sigma-Aldrich	Cat# SML1858-5MG
Benzonase® Nuclease HC	Millipore	Cat# 71206
Camptothecin	Sigma-Aldrich	Cat# 7689-03-4
Cell Event Caspase 3/7 green detection reagent	ThermoFisher Scientific	Cat# C10423
cOmplete protease inhibitor cocktail	MilliporeSigma	Cat# 4693159001
DAPI	Sigma-Aldrich	Cat# D9542-1MG
Doxorubicin hydrochloride	Sigma-Aldrich	Cat# D1515-10MG
Dynabeads M-280 streptavidin	ThermoFisher Scientific	Cat# 11205D
Dynabeads protein A for immunoprecipitation	ThermoFisher Scientific	Cat# 10001D
Dynabeads protein G for immunoprecipitation	ThermoFisher Scientific	Cat# 10009D
EcoRI-HF	New England Biolabs	Cat# R3101S
Esp3I (BsmBI) (10 U/μL)	ThermoFisher Scientific	Cat# ER0451
Fetal bovine serum (FBS)	ThermoFisher Scientific	Cat# 10082-147
HindIII	New England Biolabs	Cat# R0104
Human recombinant cleaved Caspase 3 protein	Abcam	Cat# ab52101
Human recombinant full-length PARP-1 protein	Sino Biological	Cat# 11040-H08B

(*Continued on next page*)

Continued

REAGENT OR RESOURCE	SOURCE	IDENTIFIER
Human recombinant Ku70/Ku80 protein	Sino Biological	Cat# CT018-H07B
Igepal CA-630	Sigma-Aldrich	Cat# 542334-100G-A
Lipofectamine 2000	ThermoFisher Scientific	Cat# 11668019
Lipofectamine RNAiMAX	ThermoFisher Scientific	Cat# 13778075
LIVE/DEAD fixable violet dead cell dye	ThermoFisher Scientific	Cat# L34963
n-Dodecyl β-D-maltoside	Sigma-Aldrich	Cat# D4641-1G
Neocarzinostatin from *Streptomyces carzinostaticus*	Sigma-Aldrich	Cat# 9014-02-2
Nutlin-3	Sigma-Aldrich	Cat# N6287-5MG
Opti-MEM I reduced serum medium	ThermoFisher Scientific	Cat# 11058021
Penicillin-streptomycin	ThermoFisher Scientific	Cat# 15140-163
Phenylmethylsulfonyl fluoride (PMSF)	Sigma-Aldrich	Cat# P7626
Phusion High-Fidelity DNA polymerase	New England Biolabs	Cat# M0530S
Polybrene	MilliporeSigma	Cat# H9268
Propidium iodide	Sigma-Aldrich	Cat# 81845-25MG
Proteinase K Solution, PCR grade	Roche	Cat# 03115828001
Puromycin	Sigma-Aldrich	Cat# P7255
RNase A	ThermoFisher Scientific	Cat# EN0531
RNase If	New England Biolabs	Cat# M0243S
RNaseOUT	ThermoFisher Scientific	Cat# 10777019
RNasin Plus RNase inhibitor	Promega	Cat# N2611
SafeClear Xylene Substitutes	Fisher Scientific	Cat# 23-314629
Sodium meta-arsenite	Sigma-Aldrich	Cat# S7400
SsoFast EvaGreen Supermix reagent	Bio-Rad	Cat# 1725204
Stellaris® RNA FISH Hybridization Buffer, 10 ml	Biosearch Technologies	Cat# SMF-HB1-10
Stellaris® RNA FISH Wash Buffer A, 60 ml	Biosearch Technologies	Cat# SMF-WA1-60
Stellaris® RNA FISH Wash Buffer B, 20 ml	Biosearch Technologies	Cat# SMF-WB1-20
SuperScript III Reverse Transcriptase	ThermoFisher Scientific	Cat# 18080093
SuperScript IV VILO Master Mix	ThermoFisher Scientific	Cat# 11756050
SuperSignal West Femto maximum sensitivity substrate	ThermoFisher Scientific	Cat# 34094
SYBR™ Gold Nucleic Acid Gel Stain	ThermoFisher Scientific	Cat# S11494
T4 RNA ligase 1 (ssRNA ligase)	New England Biolabs	Cat# M0204S
T7 ligase	New England Biolabs	Cat# M0318S
TaqMan® Universal PCR Master Mix no AmpErase® UNG	ThermoFisher Scientific	Cat# 4364341
Trichloroacetic acid (TCA)	Sigma-Aldrich	Cat# T0699
TRIzol	ThermoFisher Scientific	Cat# 15596026
TURBO DNase	ThermoFisher Scientific	Cat# AM2239
UltraPure™ BSA (50 mg/ml)	ThermoFisher Scientific	Cat# AM2616
VECTASHIELD antifade mounting medium	Maravai LifeSciences	Cat# H-1000
Critical commercial assays		
Alexa Fluor 647 microscale protein labeling kit	ThermoFisher Scientific	Cat# A30009
APO-BrdU TUNEL Assay kit with Alexa Fluor 488 anti-BrdU	ThermoFisher Scientific	Cat# A23210
Caspase-Glo® 3/7 Assay	Promega	Cat# G8090
CloneJET PCR cloning kit	ThermoFisher Scientific	Cat# K1231

(*Continued on next page*)

Continued

REAGENT OR RESOURCE	SOURCE	IDENTIFIER
CometAssay kit	Trevigen	Cat# 4250-050-K
Control miRNA Assay RNU6B (ID 001093)	ThermoFisher Scientific	Cat# 4427975
Dual luciferase reporter assay system	Promega	Cat# E1910
FirstChoice RLM-RACE kit	ThermoFisher Scientific	Cat# AM1700M
MEGAScript T7 transcription kit	ThermoFisher Scientific	Cat# AM1334
MinElute PCR purification kit	Qiagen	Cat# 28004
NEBNext® Ultra™ II directional RNA library prep kit for Illumina	New England Biolabs	Cat# E7760S
QIAEX II Gel Extraction Kit	Qiagen	Cat# 20021
QIAquick PCR purification kit	Qiagen	Cat# 28104
TALE Toolbox kit	Addgene	Cat# 1000000019
TaqMan® MicroRNA Assays for hsa-miR-34a-5p (ID 000426)	ThermoFisher Scientific	Cat# 4427975
TaqMan® MicroRNA Assays hsa-miR-34b-5p (ID 000427)	ThermoFisher Scientific	Cat# 4427975
TaqMan® MicroRNA Assays hsa-miR-34c-5p (ID 000428)	ThermoFisher Scientific	Cat# 4427975
TaqMan® MicroRNA Reverse Transcription Kit	ThermoFisher Scientific	Cat# 4366597
TUNEL assay kit-HRP-DAB	Abcam	Cat# ab206386
TURBO DNA-free kit	ThermoFisher Scientific	Cat# AM1907
ZymoPURE™ Plasmid Midiprep Kit (25), endo-free	Zymo Research	Cat# D4200
Deposited data		
Original images for Western blots and microscopy (Mendeley dataset)	This study	https://doi.org/10.17632/wx7t4dyjm9.1
RNA-seq	This study	GEO: GSE144510
Experimental models: Cell lines		
Human cell line: A549	ATCC	Cat# CCL-185; RRID: CVCL_0023
Human cell line: HCT116	ATCC	Cat# CCL-247; RRID: CVCL_0291
Human cell line: HCT116 $p53^{-/-}$	(Bunz et al., 1999)	N/A
Human cell line: HEK-293T	ATCC	Cat# CRL-3216; RRID: CVCL_0063
Human cell line: HepG2	ATCC	Cat# HB-8065; RRID: CVCL_0027
Human cell line: RKO	ATCC	Cat# CRL-2577; RRID: CVCL_0504
Experimental models: Organisms/Strains		
nu/nu mice	The Jackson Laboratory	Cat# 007850
Oligonucleotides		
AllStars negative control siRNA	Qiagen	Cat# 1027281
miRIDIAN microRNA Human hsa-miR-34a-5p - Mimic, 10 nmol	Dharmacon	Cat# C-300551-07-0010
miRIDIAN microRNA Human hsa-miR-34b-5p - Mimic, 10 nmol	Dharmacon	Cat# C-300654-03-0010
miRIDIAN microRNA Human hsa-miR-34c-5p - Mimic, 10 nmol	Dharmacon	Cat# C-300655-03-0010
miRIDIAN microRNA Mimic Negative Control #1, 20 nmol	Dharmacon	Cat# CN-001000-01-20
Primers and probes, see Table S3	This study	N/A
Random hexamers	ThermoFisher Scientific	Cat# N8080127
TP53 SMARTpool siRNAs	Dharmacon	Cat# L-003329-00-0005

(*Continued on next page*)

Continued

REAGENT OR RESOURCE	SOURCE	IDENTIFIER
Recombinant DNA		
Plasmid: lentiCRISPR v2	Addgene	Cat# 52961; RRID: Addgene_52961
Plasmid: pcDNA 3.1/*myc*-His A	ThermoFisher Scientific	Cat# V80020
Plasmid: pGL3-Basic	Promega	Cat# E1751
Plasmid: pSpCas9n(BB)-2A-Puro (PX462) V2.0	Addgene	Cat# 62987; RRID: Addgene_62987
Software and algorithms		
BioRender	BioRender	BioRender.com
OpenComet plugin for ImageJ	Graduate School for Integrative Sciences and Engineering, National University of Singapore and Laboratory of Systems Pharmacology, Harvard Medical School	https://cometbio.org/index.html
ImageJ	NIH	RRID:SCR_001935
Fiji v2.0.0	NIH	RRID: SCR_002285
FlowJo 8.7	FlowJo, LLC	https://www.flowjo.com/
MO.Affinity Analysis	NanoTemper Technologies	https://nanotempertech.com/monolith/
Prism 8	GraphPad	https://www.graphpad.com/scientific-software/prism/
SlideBook v4.2	Intelligent Imaging Innovations	https://www.intelligent-imaging.com/slidebook
R v3.3.3	The R project	RRID: SCR_001905; https://www.r-project.org/
hisat v2.02	CCB at JHU	http://www.ccb.jhu.edu/software/hisat/index.shtml
deepTools suite v3.3.0	(Ramírez et al., 2016)	RRID: SCR_016366; https://github.com/deeptools/deepTools
edgeR v3.12.1	(McCarthy et al., 2012)	RRID: SCR_012802; http://bioconductor.org/packages/edgeR/
Rsubread package v1.22.3	(Liao et al., 2013)	https://bioconductor.org/packages/release/bioc/html/Rsubread.html

RESOURCE AVAILABILITY

Lead contact

Further information and requests for resources and reagents should be directed to and will be fulfilled by the lead contact, Judy Lieberman, judy.lieberman@childrens.harvard.edu.

Materials availability

All unique/stable reagents generated in this study will be made available on request to the lead contact but may require a completed Materials Transfer Agreement.

Data and code availability

- The accession number for RNA-seq data reported in this paper is GEO: GSE144510. The Mendeley dataset associated to this study containing original Western blot and microscopy images can be found at DOI: https://doi.org/10.17632/wx7t4dyjm9.1
- No original code was generated in this study.
- Any additional information required to reanalyze the data reported in this paper is available from the lead contact upon request.

EXPERIMENTAL MODEL AND SUBJECT DETAILS

Cell lines and culture conditions

The human colorectal cancer HCT116, human lung adenocarcinoma A549, human hepatocellular carcinoma HepG2, human colon carcinoma RKO and HEK-293T cell lines were obtained from ATCC. p53 hypomorphic HCT116 (Bunz et al., 1999), called p53 KO in

this manuscript, were a kind gift of Dr. Bert Vogelstein, Johns Hopkins University, Baltimore, MD. Cells were cultured at 37°C in 5% CO_2 in Dulbecco's modified Eagle's medium (DMEM) (ThermoFisher Scientific) supplemented with 10% heat-inactivated fetal bovine serum (FBS), 100 U/mL penicillin G, 100 μg/mL streptomycin sulfate, 6 mM HEPES, 1.6 mM L-glutamine and 50 μM 2-mercaptoethanol (2-ME).

Animal experiments

Mouse experiments were conducted in the Harvard Medical School Animal Facility using protocols approved by the Harvard Medical School Institutional Animal Care and Use Committee (IACUC). 6-weeks-old male *nu/nu* mice (Jackson Laboratories) were subcutaneously inoculated in the flank with $3x10^6$ WT or *SPARCLE* KO HCT116 cells. Beginning fourteen days later, animals received 8 mg/kg doxorubicin (DOX) intraperitoneally weekly for four weeks. Tumor size was monitored every other day. Mice were sacrificed when any tumor in the experiment reached the maximal allowable size (100 mm^3). Excised tumors were fixed in 4% formaldehyde for 24 hr at room temperature and embedded in paraffin.

METHOD DETAILS

Cell treatments

Cells were seeded ($2.5x10^5$ cells/well) in 6-well plates overnight before each treatment. Treatment was with medium or 200 ng/mL neocarzinostatin (NCS), 1 μM doxorubicin (DOX), 50 μM nutlin-3, 4 Gy ionizing radiation (IR) administered with an RS 2000 irradiator (RadSource), 100 nM CPT or 15 μM sodium meta-arsenite. Unless otherwise indicated, treated cells were analyzed 48 hr later.

RNA extraction

RNA, isolated using TRIzol reagent (15596026, Thermo Fisher Scientific), was treated with the TURBO DNA-free kit (AM1907, Thermo Fisher Scientific) following the manufacturer's directions. RNA concentration was determined by Nanodrop (Thermo Fisher Scientific).

qRT-PCR

For small RNAs, reverse transcription (RT) reactions were performed using the TaqMan® MicroRNA Reverse Transcription Kit (4366597, ThermoFisher Scientific) in combination with the TaqMan® MicroRNA Assay (ThermoFisher Scientific) specific for each small RNA (hsa-miR-34a-5p, hsa-miR-34b-3p, hsa-miR-34b-5p, hsa-miR-34c-5p, U6). Total RNA (100 ng) was used for each RT reaction, performed according to the manufacturer's protocol. RT negative controls without enzyme or RNA were analyzed in parallel. qPCR reactions were performed using 1 μL cDNA, the specific forward primer included in the TaqMan MicroRNA Assay and the TaqMan® Universal PCR Master Mix no AmpErase® UNG (4364341, ThermoFisher Scientific) following the manufacturer's protocol using a Bio-Rad CFX96 qPCR instrument.

For larger RNAs DNAse-treated total RNA (500 ng) was used to generate cDNA using the SuperScript IV VILO Master Mix (11756050, Thermo Fisher Scientific), which contains both oligo dT and random hexamers. The PCR protocol suggested for the SsoFast EvaGreen Supermix reagent (1725204, Bio-Rad) was followed using a final volume of 20 μL, 1 μL of cDNA and 500 nM primers. All primers were designed to work using a Tm of 60°C. Primers used are listed in Table S3.

Cell cycle analysis

Treated and untreated cells were trypsinized 48 hr after genotoxic stress, washed once with 1X PBS and then permeabilized using 70% ethanol at -20°C for 1 hr. Cells were centrifuged at 5,000 rpm at room temperature for 2 min and pellets were washed twice with 1X PBS and resuspended in 100 μL 1X PBS. 1 μL of RNase A (EN0531, ThermoFisher Scientific) was added and cells were incubated at room temperature for 30 min before adding propidium iodide (PI) and incubating at room temperature for 1 hr. After adding 300 μL of 1X PBS to each sample, stained cells were analyzed on a FACSCanto II flow cytometer using FlowJo software (BD Biosciences). Differences between cell cycle profiles were analyzed by one-way ANOVA using the Holm-Sidak method and Prism software (Graphpad).

Annexin V staining

Treated and untreated cells were trypsinized 48 hr after treatment, washed once with 1X PBS and resuspended in 100 μL 1X Annexin V binding buffer (BD Biosciences), 4 μL Annexin V AlexaFluor647-conjugated antibody (A23204, ThermoFisher Scientific) and 1.8 μL LIVE/DEAD fixable violet dead cell dye (L34963, ThermoFisher Scientific). After incubation at room temperature for 30 min, 300 μL 1X Annexin V binding buffer was added to each sample. Stained cells were analyzed on a FACSCanto II flow cytometer using FlowJo software.

miRNA mimics and plasmid transfection

24 hr before any treatment, cells were transfected with 50 nM of the corresponding miRNA mimics (Dharmacon) or with 1 μg of the indicated plasmid using Lipofectamine 2000 (11668019, ThermoFisher Scientific) in Opti-MEM I reduced serum medium (11058021, ThermoFisher Scientific) following the manufacturer's suggested protocol.

Gene knockdown

24 hr before DOX treatment, cells were reverse-transfected with 20 nM of either TP53 SMARTpool siRNAs (L-003329-00-0005, Dharmacon) or the AllStars Negative Control siRNA (1027281, Qiagen) as a negative control using Lipofectamine RNAiMAX (13778075, ThermoFisher Scientific) in Opti-MEM I reduced serum medium (11058021, ThermoFisher Scientific) following the manufacturer's suggested protocol.

5' and 3' rapid amplification of cDNA ends (RACE)

5' and 3' RACE were performed using 1 μg of DNase-treated nuclear RNA from doxorubicin-treated HCT116 WT cells following the suggested protocols using the FirstChoice® RLM-RACE kit (AM1700, ThermoFisher Scientific). RACE products were purified with the QIAquick PCR purification kit (28104, Qiagen) and cloned using the CloneJET PCR cloning kit (K1231, ThermoFisher Scientific). Multiple colonies were picked and sequenced. Specific primers used for these experiments are listed in Table S3.

Circular RACE (cRACE)

20 μg of nuclear RNA from DOX-treated HCT116 WT cells was treated with TURBO DNase (AM2239, ThermoFisher Scientific) following the manufacturer's directions. Half of the DNA-free RNA was treated with 2 U of tobacco acid pyrophosphatase (TAP) for 1 hr at 37°C to remove the 5' cap, and the other half was treated the same except that TAP was not added. Reactions were then treated with 10 U of T4 RNA ligase (New England Biolabs) and 1 mM ATP in a final volume of 100 μL overnight at room temperature. RNA was ethanol precipitated, washed and resuspended in 20 μL of nuclease-free water. 3 μL of RNA were mixed with 1 μL of 10 mM deoxyribonucleotide triphosphates (dNTPs), 2 μL of the *SPARCLE* cRACE specific primer and 7 μL of nuclease-free water and then heated at 65°C for 5 min and cooled to 25°C. Then, reverse transcription was performed using SuperScript III Reverse Transcriptase (18080093, ThermoFisher Scientific) and 1 μL RNaseOUT (10777019, ThermoFisher Scientific) following the manufacturer's protocol. 2 μL of this reaction was mixed with 1 μL of each PCR primer (10 mM), 6 μL of nuclease-free water and 10 μL of the 2X Phusion polymerase mix (New England Biolabs) and amplified as follows: one cycle at 98°C for 30 s, 35 cycles at 98°C for 10 s, 60°C for 10 s and 72°C for 10 s and one cycle at 72°C for 3 min. PCR products were purified with the QIAquick PCR purification kit (28104, Qiagen) and cloned using the CloneJET PCR cloning kit (K1231, ThermoFisher Scientific). Then, multiple colonies were picked and sequenced. Gene-specific primers used for cRACE are listed in Table S3.

Luciferase assays

Cells were transfected with 1 μg of the corresponding plasmid 24 hr before treatment using Lipofectamine 2000 (11668019, ThermoFisher Scientific) following the manufacturer's suggested protocol. Treated and untreated cells were trypsinized 48 hr after genotoxic stress, washed once with 1X PBS and then lysed in 50 μL of 1X passive lysis buffer from the Dual luciferase reporter assay kit (E1910, Promega), incubated on ice for 15 min and centrifuged at 13,000 rpm at 4°C for 10 min. Supernatants were stored at -70°C before assaying luminescence of 2.5 μL of each sample using a Synergy 2 Microplate Reader (Biotek) following the manufacturer's directions. For these assays, SPARCLE's promoter was cloned into the pGL3-Basic plasmid (E1751, Promega) in forward and reverse orientation, while the deletion of individual p53REs was done by PCR and subcloning. Multiple clones were picked and verified by sequencing. Sequences of cloning primers are listed in Table S3.

Chromatin immunoprecipitation (ChIP)

Treated cells were fixed with 1% formaldehyde in fresh medium for 10 min at room temperature before adding 2.5 M glycine to a final concentration of 0.125 M to quench the reaction with gentle shaking at room temperature for 5 min. Medium was removed and cells were washed once with ice cold 1X PBS. Then 1 mL of ice cold 1X PBS was added to each 10 cm plate (around 8-9 plates per condition to get $40x10^6$ cells) and cells were scraped, collected and spun at 1,500 rpm at 4°C for 5 min. Cell pellets were resuspended in 1 mL of Solution I (10 mM Hepes pH 7.5, 10 mM EDTA, 0.5 mM EGTA and 0.75% Triton X-100) supplemented with protease inhibitors and 1 mM phenylmethylsulfonyl fluoride (PMSF) and the cOmplete protease inhibitor cocktail (4693159001, MilliporeSigma) and incubated at 4°C for 10 min with frequent turning. Nuclei were spun at 2,000 rpm at 4°C for 5 min, supernatants were discarded and pellets were gently resuspended in 1 mL of Solution II (10 mM Hepes pH 7.5, 200 mM NaCl, 1 mM EDTA and 05 mM EGTA) supplemented with PMSF and the protease inhibitor cocktail. Samples were then spun at 2,000 rpm at 4°C for 5 min, supernatants were discarded and pellets were resuspended in 1 mL of lysis buffer (25 mM Tris-HCl pH 7.5, 150 mM NaCl, 1% Triton X-100, 0.1% SDS and 0.5% sodium deoxycholate) supplemented with PMSF and the protease inhibitor cocktail and incubated on ice for 10 min. DNA shearing was performed using a sonicator with an Amplitude of 30 and 26 pulses of 30 sec with 1 min of rest intervals. Lysates were transferred to 1.5 mL tubes and spun at 13,000 rpm at 4°C for 10 min to remove cellular debris. Supernatants (chromatin in solution) were transferred to new tubes and 40 μg of chromatin were diluted in lysis buffer supplemented with PMSF and protease inhibitors in a final volume of 400 μL. 4 μL (1%) was allocated as the Input and stored at -70°C until the reverse crosslinking step to free and purify DNA. For p53 ChIP, 4 μg of p53 antibody (DO-1, sc-126, Santa Cruz Biotechnology) was added to each tube of chromatin and incubated overnight at 4°C with rotation. Then, 40 μL of protein G Dynabeads (10003D, ThermoFisher Scientific) were added and incubated for 4 hr at 4°C with rotation. Beads were pelleted using a magnet and washed for 5 min with 1 mL of each of the following buffers at 4°C with rotation: 2 washes with ChIP Wash Buffer 1 (low salt buffer: 0.1% SDS, 1% Triton X-100, 2 mM EDTA, 20 mM Tris-HCl pH 8 and 150 mM NaCl), 1 wash with ChIP Wash Buffer 2 (high salt buffer: 0.1% SDS, 1% Triton X-100, 2 mM EDTA, 20 mM Tris-HCl pH 8

and 500 mM NaCl), 1 wash with ChIP Wash Buffer 3 (LiCl buffer: 0.25 M LiCl, 1% NP40, 1% sodium deoxycholate, 1mM EDTA and 10 mM Tris-HCl pH 8) and 1 wash with TE buffer (1 mM EDTA and 10 mM Tris-HCl pH 7.5). After discarding the TE supernatant, 100 μL of ChIP Elution Buffer (1% SDS and 0.1 M $NaHCO_3$) was added and samples were mixed well. Input samples were also mixed with 100 μL of ChIP Elution Buffer. ChIP and Input samples were incubated for 1 hr at 65°C with shaking (1,200 rpm). To reverse the cross-link and elute chromatin from the beads, 4 μL of 5 M NaCl (0.2 M final concentration) was added and incubated overnight at 65°C with shaking. Beads were magnetically pelleted and supernatants were transferred to new tubes before adding 1 μL of RNase A (T3018L, New England Biolabs) and incubating at 37°C for 30 min. Then, 5 μL of proteinase K was added and the mixture was incubated at 56°C for 1 hr. DNA was purified using the MinElute PCR purification kit (28004, Qiagen) using 40 μL of the kit's elution buffer. DNA was stored at -20°C until 1 μL was used for qPCR. Primers used for this assay are listed in Table S3.

SPARCLE Taqman qPCR

DNAse-treated total RNA (1 μg) was used to generate cDNA using the SuperScript IV VILO Master Mix (11756050, ThermoFisher Scientific), which contains both oligo dT and random hexamers, in a final volume of 20 μL following manufacturer's protocol. qPCR was performed using the AmpliTaq DNA polymerase with 5' ⟍ 3'exonuclease activity (N8080166, Applied Biosystems) in a final volume of 20 μL (1 μL of cDNA, 2 μM of each forward and reverse primer, 0.4 μM of *SPARCLE* Taqman probe, 0.4 μM of dNTPs, 50 units of AmpliTaq DNA polymerase, 1x PCR buffer with pre-added $MgCl_2$ and DNase/RNase-free distilled water up to 20 μL). The cycling parameters were 95°C for 3 min and 40 cycles of: 95°C for 15 s, 60°C for 30 s and 72°C for 1 min, using a Bio-Rad CFX96 PCR machine. To calculate absolute *SPARCLE* copy numbers, the Ct values, from equal amounts of total RNA, were used to calculate copies per μg of RNA by extrapolating the copy number from standard curves performed with known amounts of *SPARCLE* plasmid (1 to 625 copies). *SPARCLE* copies per μg were converted to copies per cell assuming 20 pg of total RNA per cell. The Taqman probe and the forward and reverse primers used for this assay are listed in Table S3.

Cell fractionation

Treated and untreated cells were trypsinized 48 hr after genotoxic stress, washed once with 1X PBS and then resuspended in 300 μL of 1X PBS plus 300 μL of 0.1% Igepal and immediately spun at 6,000 rpm for 15 s at room temperature. Supernatants were saved as cytoplasmic fractions and stored at -70°C until protein quantification or processed for RNA extraction using TRIzol. Nuclear pellets were then gently resuspended in cold 0.05% Igepal and spun at 6,000 rpm for 15 s at room temperature. Supernatants were discarded to eliminate cytoplasmic contamination. For RNA extraction, TRIzol (15596026, ThermoFisher Scientific) was directly added and samples were processed following manufacturer's directions. To extract nuclear proteins, pellets were resuspended in 50 μL of lysis buffer supplemented with 1 mM PMSF and the cOmplete protease inhibitor cocktail (4693159001, MilliporeSigma), incubated on ice for 15 min and spun at 13,000 rpm at 4°C for 10 min. Supernatants were saved as nuclear fractions and stored at -70°C until protein quantification.

Immunoblot

Cells were lysed in lysis buffer (50 mM Tris-Cl pH7.4, 150 mM NaCl, 1% Triton X-100) supplemented with 1 mM PMSF and the cOmplete protease inhibitor cocktail (4693159001, MilliporeSigma). Protein concentration was determined by using the Pierce BCA protein assay (ThermoFisher Scientific). 7 μg of protein in cell lysates was added to SDS loading buffer (50 mM Tris-HCl pH 6.8, 10% glycerol, 2% SDS, 1% 2-mercaptoethanol and 0.1% bromophenol blue), boiled for 5 min, analyzed by SDS-PAGE and transfer to Immobilon-P PVDF membranes (IPVH00010, MilliporeSigma), which were then blocked with 5% milk in TBS-T buffer (150 mM NaCl, 20 mM Tris-HCl pH 7.6, 0.05% Tween-20) for 1 hr before overnight incubation with primary antibody at 4°C. After three washes of 5 min with TBS-T, membranes were incubated with secondary antibody for 1 hr at room temperature and then washed three times with TBS-T before adding the SuperSignal West Femto maximum sensitivity substrate (34094, ThermoFisher Scientific) for chemiluminescent detection. Antibodies used were PARP-1 (B-10, sc-74470, Santa Cruz Biotechnology), Ku80/Ku86 (B-1, sc-5280, Santa Cruz Biotechnology), lamin A (E-1, sc-376248, Santa Cruz Biotechnology), caspase-3 ([ABM1C12], ab208161, Abcam), β-actin (JLA20-c, Developmental Studies Hybridoma Bank) and α-tubulin (T5168, Sigma).

Single-molecule FISH (smFISH)

Single-molecule RNA fluorescence in situ hybridization (FISH) for *SPARCLE* was performed using a pool of 23 Quasar® 570 single-labeled probes designed and purchased from Stellaris Biosearch Technologies following the manufacturer's directions, except for substituting a 72 hr incubation time for the hybridization step. Cells were imaged using an Axiovert 200M microscope (Pan Apochromat, 1.4 NA; Carl Zeiss) at 63X. Images were analyzed with SlideBook 4.2 software (Intelligent Imaging Innovations). All images shown are representative of at least three independent experiments.

SPARCLE truncations

Full-length *SPARCLE*, *SPARCLE* fragments and the reverse sequence of the first 275 nt of *SPARCLE* (*ELCRAPS*) were amplified by PCR using the Phusion High-Fidelity DNA polymerase (M0530S, New England Biolabs) following the manufacturer's protocol and subcloned into the pcDNA3.1 plasmid (V80020, ThermoFisher Scientific). Multiple clones were picked and verified by sequencing. Primer sequences are listed in Table S3.

PARP-1 N-terminal domain (PARP-1-NT) cloning

The PARP-1 N-terminal domain expression vector was generated by PCR amplification using the Phusion High-Fidelity DNA polymerase (M0530S, New England Biolabs) following the manufacturer's protocol and subcloned into the NotI and XhoI sites of the pcDNA3.1(+)/myc-His A plasmid (V80020, ThermoFisher Scientific). Multiple clones were picked and correct cloning was verified by sequencing. Primer sequences are listed in Table S3.

Generation of miR-34b/c KO and p53RE2 KO HCT116 cells using TALENs

To remove miR-34b/c or p53RE2, TALENs were designed to disrupt the sequence of each of these loci in HCT116 cells. TALENs were generated using the TALE Toolbox kit (1000000019, Addgene). Cells were transfected with 2 μg of each TALEN using Lipofectamine 2000 (11668019, ThermoFisher Scientific) and plated by limiting dilution in 100 mm dishes 48 hr post-transfection. Single clones were tested for miR-34b/c or p53RE2 sequence by qPCR and edited clones were verified by sequencing.

Generation of *SPARCLE* KO HCT116, A549 and HepG2 cells using CRISPR/Cas9

To generate *SPARCLE* KO HCT116 cells lacking the first 275 nt of *SPARCLE*, two sgRNAs (sgRNA 1 and sgRNA 2) flanking this genomic region were independently cloned into the pSpCas9n(BB)-2A-Puro (PX462) V2.0 plasmid (62987, Addgene).

For generating *SPARCLE* KO A549 and HepG2 cells, the lentiCRISPR v2 plasmid (52961, Addgene) was used to generate a single cut that leads to random and different-sized deletions within the *SPARCLE's* region complementary to each designed sgRNA. Cells were infected (A549, HepG2) or co-infected (HCT116) with the corresponding lentivirus derived from the corresponding constructs in 35 mm dishes and selected with 2 μg/mL puromycin (P7255, Sigma) for two weeks and cloned by seeding one cell per well in 96-well plates. Clones were analyzed by sequencing and qPCR, and 2 or 3 independent clones were selected. Although two versions of the CRISPR/Cas9 system were used to generate *SPARCLE* KO cell lines in this study and 250-300 clones were screened for each CRISPR experiment and cell line, only 2-3 complete KO clones were found for each cell line. This suggests that the genomic locus of *SPARCLE* may have inherent unknown characteristics that make gene editing challenging within this region. sgRNA sequences are listed in Table S3.

RNA-seq libraries and sequencing

RNA from untreated or 48 hr DOX-treated WT, *SPARCLE* KO (KO), or *SPARCLE* KO over-expressing *SPARCLE* (OE) HCT116 cells was isolated following the TRIzol protocol (15596026, ThermoFisher Scientific). Illumina RNA-seq libraries were obtained from 500 ng of total RNA using the NEBNext® Ultra™ II Directional RNA Library Prep Kit for Illumina (E7760S, New England Biolabs) following the manufacturer's instructions. Libraries were quality controlled, pooled and sequenced in a NextSeq 550 using the high-output mode.

RNA antisense purification-mass spectrometry (RAP-MS)

Treated and untreated WT and *SPARCLE* KO HCT116 cells seeded in 150 mm plates were UV-crosslinked and processed for RAP-MS experiments 48 hr post-treatment as described (McHugh et al., 2015). Briefly, UV-crosslinked cells ($40x10^6$ per condition) were collected to prepare nuclear lysates. Lysates were pre-cleared and then, incubated with 5 μg of each of the three *SPARCLE* spanning biotinylated probes (Table S3) for 2 hr at 67°C with intermittent shaking at 1,100 rpm (30 s shaking, 30 s off). Lysates were incubated with pre-cleared, streptavidin-coated Dynabeads M-280 (11205D, ThermoFisher Scientific,) for 30 min at 67°C with intermittent shaking (30 s shaking, 30 s off). Beads were washed and proteins were eluted using 125 U of benzonase (71206, Millipore). Finally, proteins were precipitated using 10% trichloroacetic acid (TCA) (T0699, Sigma) overnight at 4°C. The next day samples were spun at 13,000 rpm for 30 min to pellet proteins, washed once with 1 mL of cold acetone and spun again at 13,000 rpm for 15 min at room temperature. Supernatants were discarded and protein pellets were air-dried before mass spectrometry analysis at the Taplin Mass Spectrometry Facility, Harvard Medical School.

RNA immunoprecipitation (RIP)

After 48 hr of DOX treatment, both treated and untreated cells were harvested by trypsinization from eight 100 mm plates and washed once with ice-cold 1X PBS. After 5 minutes 5,000 rpm centrifugation, pellets were collected and resuspended in 2 mL of nuclear isolation buffer (1.28 M sucrose, 40 mM Tris-HCl pH 7.5, 20 mM $MgCl_2$ and 4% Triton X-100) mixed with 6 mL of RNase-free water. Lysates were incubated at 4°C for 20 minutes with frequent mixing. To complete nuclei isolation and the lysis of nuclear pellets, cells were spun at 5,000 rpm for 5 min and then resuspended in 1 mL of RIP buffer (150 mM KCl, 25 mM Tris pH 7.4, 5 mM EDTA, 0.5 mM DTT, 0.5% NP-40) freshly supplemented with 200 U/mL of the RNasin Plus RNase inhibitor (N2611, Promega) and 1X cOmplete protease inhibitors cocktail (4693159001, MilliporeSigma). Chromatin from isolated nuclei was sheared using a sonicator with the next settings: Amplitude 30, 20 pulses of 30 seconds with 1 min rest between them. Sonicated samples were spun at 13,000 rpm at 4°C for 10 min and supernatants were split into two 500 μL aliquots (one for the input and the rest for the immunoprecipitation (IP) step). Input aliquots were stored at -80°C until RNA extraction was performed. IP samples were incubated with 8 μg of either PARP-1 antibody (B-10, sc-74470, Santa Cruz Biotechnology) or Ku80/Ku86 antibody (B-1, sc-5280, Santa Cruz Biotechnology) at 4°C overnight with gentle rotation. Next day, 40 μL of protein A or G Dynabeads (10001D/10009D, ThermoFisher Scientific) were added and incubated at 4°C for 1 hour. To wash unbound material, beads were pelleted at 2,500 rpm for 30 seconds and supernatant was removed. Beads were resuspended in 500 μL of RIP buffer and a total of three RIP washes followed by one 1X PBS wash, were performed. To isolate

coprecipitated RNAs, beads and inputs were mixed with TRIzol and total RNA was extracted following the manufacturer's protocol. *SPARCLE* KO cells were used as negative control for these experiments.

TUNEL assay

Untreated and 48 hr DOX-treated WT and *SPARCLE* KO HCT116 cells were processed following the protocol of the APO-BrdU TUNEL Assay kit (A23210, ThermoFisher Scientific) and fluorescence of cells was analyzed on a FACSCanto II flow cytometer using FlowJo software.

COMET assay

WT and *SPARCLE* KO HCT116 cells treated with DOX for indicated times were processed to perform alkaline COMET assay following the protocol of the CometAssay kit (4250-050-K, Trevigen). Fluorescence images were acquired using a Zeiss 800 laser scanning confocal microscope at 20x magnification and analyzed using Zeiss Zen software. At least 50 cells were analyzed for each condition. DNA damage in COMET assay images was analyzed using the OpenComet plugin for ImageJ and reported as tail moment, which combines measurements of the amount of DNA in the tail with the distance it has migrated.

HR and NHEJ reporter assays

DNA double strand break (DSB) repair was assessed using HR and NHEJ reporter plasmids as described (Seluanov et al., 2010). Briefly, reporter plasmids, digested with HindIII (R0104, New England Biolabs), were co-transfected with 1 μg of the first 275 bp of *SPARCLE* (*SPARCLE 275*) expression plasmid into HCT116 WT cells as linear DNA using 0.5 μg of the linearized NHEJ reporter plasmid or 2 μg of the linearized HR reporter plasmid. Cells were analyzed on a FACSCanto II flow cytometer using FlowJo software 3 days later.

Immunofluorescence

WT or *SPARCLE* KO HCT116 ($7x10^5$), seeded onto 18 mm circular glass coverslips (18CIR-1, ThermoFisher Scientific) were treated with indicated DNA damaging agents for 48 h and then washed once with 1X PBS and fixed with 3.7% formaldehyde at room temperature for 10 min. Cells were washed twice with 1X PBS and permeabilized with 0.5% Triton at room temperature for 10 min. Permeabilized cells were washed once with 1X PBS and then blocked using IF buffer (5% BSA, 0.1% Triton X-100 in PBS) at room temperature for 30 min. Primary anti-phosphohistone H2A.X (Ser139) (γH2A.X, 9718S, Cell Signaling) at 1:500 was incubated overnight at 4°C with gentle shaking. After 3 washes with 0.05% TBS-T, the goat anti-rabbit IgG (H+L) highly cross-adsorbed Alexa Fluor 488 secondary antibody (A-11034, ThermoFisher Scientific) added at 1:1000 in DAPI-containing IF buffer was incubated at room temperature in the dark for 1 hr. Washed coverslips were mounted onto glass slides using VECTASHIELD antifade mounting medium (H-1000, Maravai LifeSciences). Fluorescence images were acquired using an Axiovert 200M microscope (Pan Apochromat, 1.4 NA; Carl Zeiss) and analyzed using SlideBook 4.2 software (Intelligent Imaging Innovations).

In vitro transcription

2 μg of linearized plasmid encoding full-length *SPARCLE* (*SPARCLE 3K*), the first 75 nt (*SPARCLE 75*), 178 nt (*SPARCLE 178*) or 275 nt (*SPARCLE 275*) of *SPARCLE* sequence or the reverse sequence of *SPARCLE 275* (*ELCRAPS*) were *in vitro* transcribed using the MEGAScript T7 transcription kit (AM1334, ThermoFisher Scientific) following the manufacturer's directions, but with increased incubation time (6 hr).

PARP-1 *in vitro* cleavage

50 ng of human recombinant full-length PARP-1 protein (11040-H08B, Sino Biological) were incubated at 37°C for 10 min with 0.5 units of human recombinant cleaved Caspase 3 protein (ab52101, Abcam) and with the indicated amount of *in vitro* transcribed *SPARCLE 75*, *SPARCLE 178*, *SPARCLE 275* or *ELCRAPS*. Cleavage products were detected by immunoblot using an antibody that recognizes full-length and N-terminal PARP-1 (B-10, sc-74470, Santa Cruz Biotechnology).

Microscale thermophoresis (MST)

Human recombinant PARP-1 (11040-H08B, Sino Biological) or Ku70/Ku80 protein (CT018-H07B, Sino Biological) were labeled with Alexa647 using the Alexa Fluor 647 microscale protein labeling kit (A30009, ThermoFisher Scientific). 25 nM of Alexa647-labeled PARP-1 or Ku70/Ku80 in MST buffer (50 mM HEPES, 150 mM NaCl, 0.05% Tween20) were mixed with 0 or 120 nM of *in vitro* transcribed *SPARCLE* or *ELCRAPS* RNA and incubated at room temperature for 30 min to achieve binding equilibrium. Reaction mixtures were taken up into MST capillaries and measurements were acquired using a Monolith NT.115 (NanoTemper Technologies). Data were fit using the Hill equation and K_D values were determined using the MO.Affinity analysis software (NanoTemper Technologies, Munich, Germany).

PARP-1 inhibition

Seeded HCT116 cells were incubated with medium or NCS and DMSO or 10 μM Olaparib (PARP-1 inhibitor) and analyzed 48 hr later for annexin V staining by flow cytometry.

Caspase-3 activity assay

To measure caspase-3 activity, cells were trypsinized 48 hr after indicated treatment, washed once with 1X PBS and resuspended in 500 μL of 1X PBS containing 0.5 μL of the CellEvent Caspase-3/7 green detection reagent (C10423, Thermo Fisher Scientific) and 1.8 μL LIVE/DEAD fixable violet dead cell dye (L34963, ThermoFisher Scientific). After 35 min incubation at 37°C, stained cells were analyzed on a FACSCanto II flow cytometer using FlowJo software.

TUNEL immunohistochemistry

Slides of paraffin-embedded sections of WT- and *SPARCLE* KO-HCT116 cells-derived tumors were assessed for TUNEL using the TUNEL assay kit-HRP-DAB (ab206386, Abcam) following the manufacturer's protocol, except for substitution of xylene with Safe-Clear Xylene Substitutes (23-314629, Fisher Scientific) for sample rehydration and counterstaining. TUNEL signal was analyzed using an Eclipse TE300 inverted microscope (40X, Nikon).

QUANTIFICATION AND STATISTICAL ANALYSIS

Quantification

ImageJ software was used to quantify signal intensities of bands in western blots, the number of foci in immunofluorescence microscopy slides and TUNEL+ tumor cells in immunohistochemistry slides and the tail moment of COMET assays.

Statistics

Data are presented as mean ± standard error. Kolmogorov-Smirnov normality tests were applied to the data. For multiple paired comparisons, student's t-tests were used to determine p-values, except for cell cycle analysis, survival curves and tumor size comparisons where differences were analyzed by one-way ANOVA using the Holm-Sidak method. QuickCalcs and Prism softwares (Graphpad) were used to perform all the statistical tests. p-values <0.05 were considered significant.

RNA-seq analysis

RNA-seq reads were aligned against the human transcriptome (Ensembl v85 annotation) with HISAT 2.02 using the following parameters: –no-unal –rna-strandness R. Alignments with QS <10 or falling within Encode blacklisted regions were eliminated. Coverage bigwig files were generated with the bamCoverage program from the Deeptools suite v3.3.0. Read count tables were obtained with featureCounts from the Rsubred package v1.22.3 in a R 3.3.3 environment with the following parameters: allowMultiOverlap=T, largestOverlap=T, strandSpecific=2. The read count table was analyzed with edgeR v3.12.1. After deleting poorly expressed genes (cpm<1), calculating normalization factors, and estimating dispersion, differentially expressed genes between treated/untreated WT, KO and OE cells were calculated using glm modeling. A gene was considered to be differentially expressed if it had a $\log_2$ fold change > 1 and a FDR <1e-5.